SYNTHESIS OF CYSTEINE COATED-FERRITE NANOPARTICLES - STUDY OF ADSORPTION OF CERTAIN HAZARDOUS METAL IONS ON THEIR SURFACE

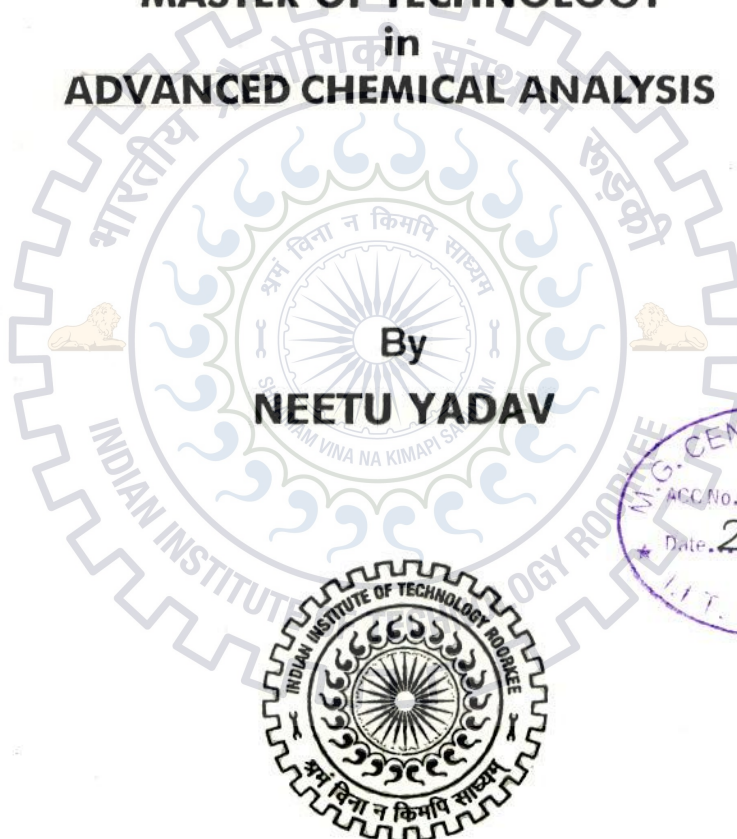## A DISSERTATION

Submitted in partial fulfillment of the
requirements for the award of the degree
of
MASTER OF TECHNOLOGY
in
ADVANCED CHEMICAL ANALYSIS

By

NEETU YADAV

DEPARTMENT OF CHEMISTRY
INDIAN INSTITUTE OF TECHNOLOGY ROORKEE
### ROORKEE -247 667 (INDIA)
JUNE, 2013

CANDIDATE DECLARATION

I hereby, certify that the work which has been presented in this dissertation entitled

"SYNTHESIS OF CYSTEINE COATED - FERRITE NANOPARTICLES - STUDY OF ADSORPTION OF CERTAIN HAZARDOUS METAL IONS ON THEIR SURFACE"

submitted in partial fulfillment for the award of degree of **Master of Technology** in **"Advanced Chemical Analysis"** submitted in the **Department of Chemistry, Indian Institute of Technology, Roorkee**, is an authentic record of my own work carried by me under the supervision of **Prof. Anil Kumar**, Department of Chemistry, Indian Institute of Technology, Roorkee.

Date: 17/06/13

Place: Roorkee

Neetu Yadav

Neetu Yadav

Certificate
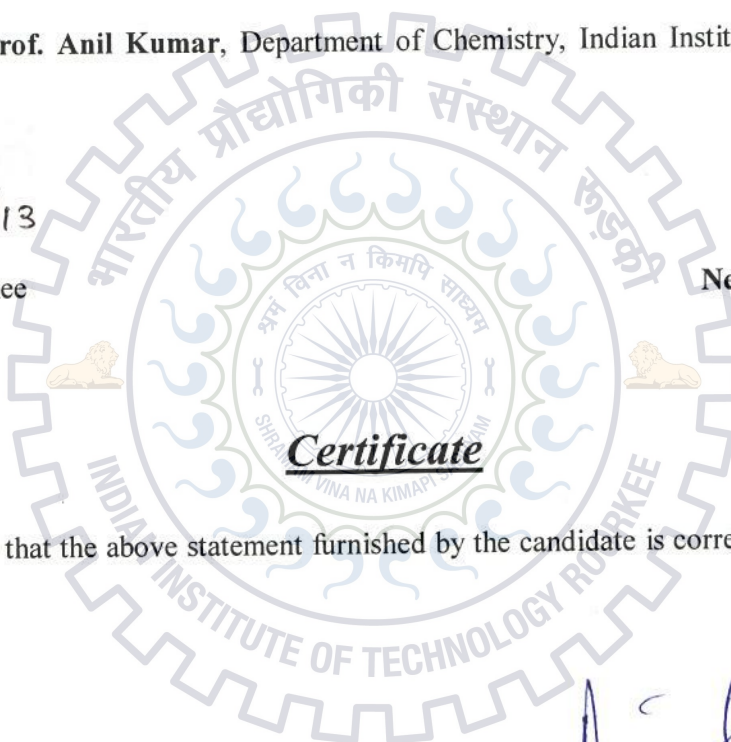
This is to certify that the above statement furnished by the candidate is correct to the best of my knowledge.

Dr. Anil Kumar

18/06/13

Professor and Head

Department of Chemistry

IIT Roorkee

i

Acknowledgement

CONTENTS

ABSTRACT

In the present work we have synthesized Fe_3O_4 and cysteine coated - Fe_3O_4 by co-precipitation process and characterized them by XRD, FE-SEM, AFM, TEM, FT-IR, UV-VIS, TGA-DTA-DTG, Zeta-probe and VSM techniques. The particle size of cysteine coated - Fe_3O_4 was estimated at about 12 nm and was supported by SEM, AFM and TEM studies. TEM study indicates that in the cysteine coated - Fe_3O_4 nanoparticles are present in the core. The coating of cysteine also indicates by EDAX analysis in FE-SEM, FT-IR and UV-Visible spectroscopy. Zeta probe shows the negative charge on coated nanoparticles. Both Fe_3O_4 and cysteine coated - Fe_3O_4 exhibit superparamagnetic behavior and the magnetization (emu/g) of the coated particles is decreased to 66.8 emu/g as compare to 74.1 emu/g for the bare Fe_3O_4 nanoparticles. As synthesize cysteine coated - Fe_3O_4 nanoparticles were used for the adsorption of environmentally toxic Pb^{+2}. Capacity of adsorption of Pb^{+2} was estimated at 33.5 mg/g and the metal recovery could be achieved up to 82.5 ± 7.5 %. This system could be utilized for the removal of other toxic ions as well.

LIST OF FIGURES

LIST OF TABLES

General Introduction

In modern age, nanoscience has emerged as one of the most powerful branch of science finding tremendous interdisciplinary applications. The use of nanomaterials endeavors many advantages because of their exclusive size and unique physiochemical properties. Nanoscience investigates the nature of matter between atoms, molecules (defined by quantum mechanics) and condensed matter (defined by solid state chemistry / Physics).

The concept of seeded nanotechnology was first discussed in 1959 by eminent physicist **Richard Feyman** in his talk. The term "nanotechnology" was first used by **Norio Taniguchi**. After the discovery of fullerenes (C_{60}) in 1980's the term nanotechnology came into the limelight.

Nanomaterial at the atomic, molecular, and supramolecular levels becomes important in the length scale of approximately 1-100nm range. An important idea that underpins much of nanotechnology is that by controlling composition, size, shape and structure at the nanoscale, which could be used to manipulate their physiochemical behavior[1].

A lot of research has been contributed in the area of nanosciences over the last two decades. By reducing the dimension one can produce 1D, 2D and 3D nanostructures i.e thin flim, nanowires and dots respectively. Scientist synthesized different nanomaterials like carbon nanotubes, silver ions, zero-valent iron, quantum dots, nanoclusters (semiconductor cores, metallic cores), metal oxides nanoparticles (iron, cobalt, nickel, zinc), metal nanoparticles (gold, palladium, platinum, copper), semiconductor (CdSe, CdS, cadmium chalcogenides)[2]. Nanomaterials have far larger surface areas than similar volumes of larger – scale materials, meaning that more surface is available for interaction with other materials around them. The size

and shape of the nanoparticles depends on their environment, temperature and how they are fabricated.

In nanosized materials, the phenomenon of quantum confinement controls their properties. Normally, bulk Au nanoparticles does not work as catalyst but in nano domain it demonstrates catalytic activity and iron oxide also splashes the superparamagnetic behavior in nano region. Nanoparticles have also the nontrivial size effect that can be important for chemical reactivity. There are various factors which controls the chemical activity of nanoparticles or nanoparticles supported on the matrix such as: geometrical, electronic and chemical.

Now, a clearer picture is emerging about designing of nanoscale material with desired properties and these materials are finding increasing in the field of medicine application, electronic, environment, water treatment and other commercial products[3-4]. As regards to their usage in medicine, silver ions are used as an anti-microbial material which inhibit or reduce the growth of microbes and are also used in food and cosmetic products to check the growth of harmful microbes. Like this, carbon nanotube is used in the airways for test rodent. Nanoscale zero-valent iron used as cleaner product for carcinogenic material like arsenic, lindane and trichloroethylene. Nanoparticles of cerium oxide are added to the diesel fuel to decrease the toxin emission and increase the fuel efficiency[5].

In all nanoscale material, magnetic nanoparticles have excessive consideration due to their magnetic property. The iron oxide based ferrite nanoparticles are used in this work; they are functionalized with amino acid (Cysteine) and are used in study of adsorption of certain hazardous metals.

CHAPTER - 1

INTRODUCTION

Iron oxide is found in nature in various forms such as hametite (α- Fe_2O_3), wüstite (FeO), β- Fe_2O_3, maghemite (γ - Fe_2O_3), goethite (α - FeOOH), magnetite (Fe_3O_4) and ε- Fe_2O_3. In all the ferrites, magnetite has drawn great attention in the field of biomedical applications because of their magnetic nature, less toxicity, biodegradability and bio-compatibility[6]. Magnetite nanoparticles shows the super-paramagnetic behavior at the nano level. Synthesis of magnetite with appropriate surface modification has been used for different applications such as diagnosis[7], hyperthermia[8], drug delivery[9], , sensors[10], catalysis[11], waste water treatment[12] terabit magnetic storage device, tissue repair, MRI contrast enhancement[13] and immunoassay. Magnetite nanoparticles have been functionalized with different organic materials or bio-molecules like PEG[14], PVP[15], humic acid[16], chitosan[17], dendrimer[18], gum arabic[19], silica[20], starch[21], poly (amino acid)[22], proteins[23], nucleic acid respectively and on modification these nanoparticles shows different distinctive properties useful for different applications[24]. Functionalized iron oxide nanoparticles avoid the agglomeration of the nanoparticles and increases in their stability. There are many methods to synthesize the magnetite nanoparticles such as:

1. Co-precipitation,

2. Thermal decomposition,

3. Micro emulsion,

4. Sol-gel,

5. Hydrothermal method.

1. **Co-precipitation method:** The co-precipitation method for synthesis of iron oxide nanoparticles is related to the stoichiometric ratio of the ferrous and ferric ion and this method consists of mixing of Fe^{+3}/ Fe^{+2} in 2:1 molar ratio in highly alkaline aqueous medium under inert environment. Size and properties of iron oxide nanoparticles depends on the temperature, pH, and ionic strength of the media. In all these conventional methods the co-precipitation method is the easiest and cheapest method.

2. **Thermal Decomposition:** In this method an organic solution phase decomposition route is used. This method consists of different salts of iron like iron (II) oleate, Fe (Cup)$_3$, Fe (CO)$_5$, Fe (acac)$_3$ in non aqueous medium for thermal degradation with the surfactant such as fatty acids, oleic acid and hexadecylamine. The size and morphology of the nanoparticles depends on the ratios of the starting organometallic compound, surfactant and solvent. This method produces highly monodispersed nanoparticles[25].

3. **Micro-emulsion method:** The microemulsion is the mixture of two immiscible liquids which are thermodynamically stable isotropic dispersion. In this method, two emulsions are mixed in the surfactant and at last in the micelles the precipitate is formed. For example - firstly microemulsion is prepared by dissolving cetyltrimethylammonium bromide (CTAB) in n-octane followed by heptanol. The resultant solution is stirred. Second microemultion consists of CTAB / heptanol / octane and both microemulsions were mixed in equal amount with stirring and finally the precipitate is formed in the micelles. This precipitate will separate out by the solvent such as ethanol or acetone. Many nanoparticles like gold-coated cobalt, metallic cobalt and cobalt/platinum alloys have been synthesized by using the microemulsion technique. Nanoparticles have been

synthesized by formation of the reverse micelles of where the oil phase and co-surfactant are octane and 1-butanol respectively[26].

4. **Sol-gel method:** The sol-gel process is a wet-chemical method and broadly used for the fabrication of materials in the field of materials science and ceramic engineering. In this method the chemical solution behaves like a precursor for making gel. Metal alkoxides and metal chlorides are mostly used as the precursor and these precursors undergo hydrolysis and poly-condensation reaction in making gel. By this the sol is generated towards the formation of gel which contain two phases (liquid and solid phase) system. For the phase separation centrifuge can also be used. Many nanoparticles can be synthesized by this process. Many researchers used these methods for the synthesis of ferrites nanoparticles[27].

5. **Hydrothermal method:** Using hydrothermal method a wide range of nanomaterials can be produced. This system consists of a solid phase (metal linoleate) and a liquid phase (ethanol-linoleic acid) in the solution (water - ethanol) interacting at different temperature under ambient conditions. For example, iron oxide nanoparticles were synthesized by mixing a predefined amount of $FeCl_3$, ethylene glycol, sodium acetate, polyethylene glycol and stirred for 8-72 hr at 200 $^{\circ}$C [28].

There are various applications of zero - valent iron and magnetite nanoparticles. Zero-valent iron is used in the water filtration technique[29]. Iron oxides are used efficiently in waste water treatment. Superparamagnetic iron oxide nanoparticles have been used in removal of heavy metals like cadmium, mercury, lead, copper, zinc, arsenic and nickel [30-32]. These heavy metals are toxic and carcinogenic in nature. A number of methods have been used for the removal of heavy metals such as adsorption, filtration, reverse osmosis, chemical separation and

membrane separation. In all these methods, adsorption is one of the most feasible and tried methods for removing the trace metals from the aqueous solutions[33].

Wang et al.[34] used the amino functionalized Fe_3O_4®SiO_2 magnetic nanoparticles with the core- shell structure in the removal of heavy metals Cu(II), Cd(II), Pb(II) from the aqueous solution.

Ge et al.[35] prepared the acrylic acid and crotonic acid co-polymer coated Fe_3O_4 nanoparticles which were modified by 3-aminopropyaltriethoxysilane and the adsorption capacity of these nanoparticles were studied by adsorption isotherm. The thermodynamics and kinetic study of the nanoparticles were also studied. Cd^{+2}, Zn^{+2}, Pb^{+2}, Cu^{+2} were removed by the use of these nanoparticles from aqueous solution.

Chen et al.[36] functionalized the boron nitride nanotubes with Fe_3O_4 nanoparticles by ultra-sonication and used in the removal of As (V) from water. They measured the Langmuir, Freundlich and Dubinin-Radushkevich adsorption isotherms. In this these nanotubes were used as adsorbent in water.

Badruddoza et al.[37] synthesized the Fe_3O_4 nanoparticles functionalized with carboxymethyl β-cyclodextrin and used as nano-adsorbent for the removal of copper ion from aqueous solution as well as adsorption studies were also analyzed.

Another researcher **White et al.**[38] used the commercially available γ-Fe_2O_3 nanoparticles for metal chelation. Those nanoparticles were functionalized with poly L-cysteine by using some organic molecule (3-aminopropyltryethoxysilane and gluteraldehyde) as linkers. The adsorption capacity of these particles on the metals like As(II), Cd(II), Pb(II), Cu(II), Zn(II), Ni(II) were

Ni(II) were studied and compared with the adsorption capacity of un-functionalized γ-Fe$_2$O$_3$ nanoparticles. Functionalized γ-Fe$_2$O$_3$ nanoparticles were found to have greater adsorption capacity than un-functionalized nanoparticles.

Cysteine: Funtionalized Materials

Cysteine is the naturally occurring amino acid which shows the hydrophilic nature and has antioxidant properties. It is biocompatible and less toxic in nature. Among all amino acids, cysteine (Cys) has three functional groups; sulphydral (-SH), carboxylic group (-COOH) and amino group (-NH$_2$) having different characterstics. The structure of cysteine is,
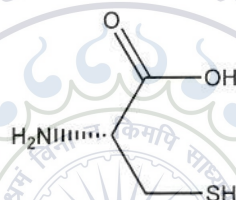
Figure 1. Structure of Cysteine (2-amino-3-sulphydrylpropanoic acid).

Cysteine has high metal binding capacity and is known to be among one of the best metal chelators. The thiol group has high affinity for heavy metals, so proteins containing cysteine, will binds heavy metals like mercury, lead, arsenic and cadmium tightly. Cysteine easily binds to the magnetite nanoparticles with thiol and carboxyl group by forming hydrogen bond, the amino group remains free in this interaction[39].

Figure 2: Shows the interaction between magnetite and cysteine molecule

Some researchers used cysteine coated magnetic nanoparticles in different applications like MRI contrast enhancement and as catalyst[40].

In today's world increasing industrialization has created a serious problem is environmental pollution and due to this increased pollution has an adverse effect on both human being and living organism. Chemical pollution includes both organic and inorganic pollutants. Among inorganic pollutants Pb, Hg and As are extreme hazardous. Pb is very poisonous for brain cell function and neurobehavioral development even in trace amount. Lead pollution arises due to the disposal of lead containing batteries, sewage waste and use of gasoline antilock product, paint pigments, fertilizers and pesticides[41]. The removal of lead from the aqueous solution by adsorption process is very convenient then other processes.

Here in this work the cysteine coated ferrites are used for adsorption of lead from aqueous solution.

AIM AND SCOPE OF MY WORK

In view of the above literature survey, the aim and scope of present work is to synthesize the bare and cysteine coated nanosized ferrite (magnetite) using co-precipitation method. The synthesized nanomaterials will be characterized in terms of their size, morphology, charge, structure and magnetic properties. Advanced analytical techniques like SEM, TEM, XRD, VSM, AFM, FT-IR, UV-Visible, thermal analysis and Zeta probe would be employed for their characterization. The functionalized nanosystem will be explored for the study of adsorption of Pb^{+2} ions from aqueous solution. The adsorption capacity will be determined by using atomic absorption spectroscopy.
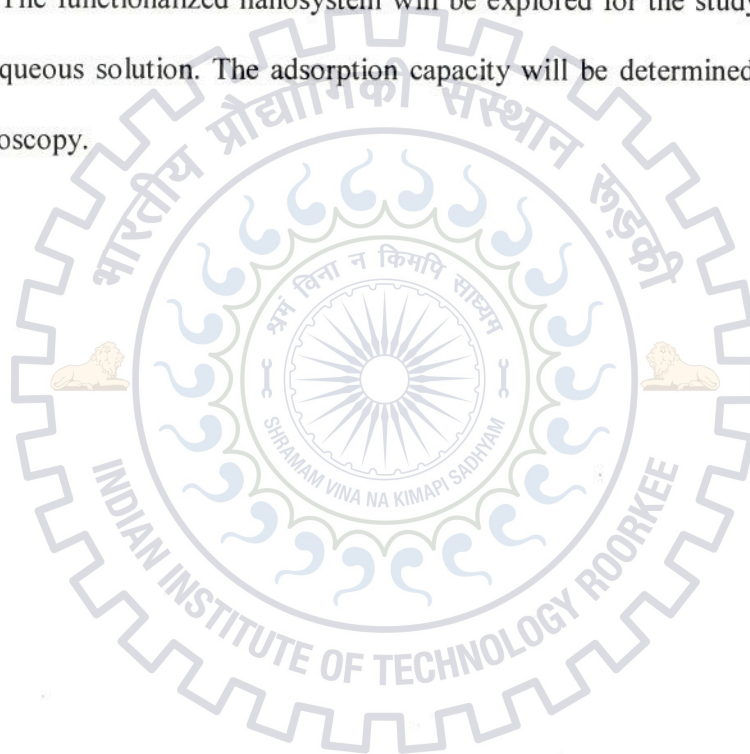
CHAPTER – 2

TOOLS AND TECHNIQUES

Experimental Section

Experimental section will be described in the following section:-

(i)   Chemicals / Reagents used

(ii)   Equipment

(iii)   Methods used

(iv)   Characterization techniques

2.1   Chemicals / Reagents

All the chemicals which were used in the experimental work were of analytical grade and were used without further purification. Deionized ultrapure water (Millipore, Specific resistivity 18.2MΩ, 25 °C) was used in all sample preparations.

Chemical name	Supplier
Anhydrous ferric chloride	Merck
Ferrous sulfate heptahydrated	Merck
Cysteine	Aldrich chem.
Sodium hydroxide	Thomas braker
Ethanol	Merck
Lead nitrate	Thomas braker
Sodium acetate	Merck
Acetic acid	Merck

2.2   Equipment:

Different advanced analytical techniques were used such as XRD, VSM, UV-Visible, AFM, FE-SEM, TEM, Zeta Potential and FT- IR and TGA-DTA-DTG for the characterization of the coated and non-coated magnetite nanoparticles. AAS technique was used to study the adsorption of hazardous metal ions (Pb^{+2}) on the surface of these nanoparticles. The basic principle of above mentioned techniques are explained below briefly:

2.2.1   X-RAY DIFFERACTION (XRD)

X-ray diffraction is a tool for the investigation of the fine structure of matter. In this technique, the high energy x-rays are produced by the transition of an electron in an atom from one orbit to another orbit. This technique provides information about the phase, crystallinity, size and information about the unit cell dimension.

2.2.1a Basic principle:

XRD depends on the constructive interference of monochromatic X-rays. The basic phenomenon of the x-ray diffraction is that the parallel incident radiations are fall on the material and reflected from the planes at angle θ, to produce the diffraction pattern of the material; here the planes are separated by the distance of d. The interaction between the incident radiation and reflected rays is represented by the Bragg's equation

$$n\lambda = 2d\ sin\theta$$

Where   n→1, 2, 3, 4, 5……is the order of reflection

λ→ wavelength of incident radiation in nm

d → distance between the two planes,

θ → Bragg's angle

2.2.1b X-ray diffractometer

An X-ray diffractometer has mainly three components: X- ray tube, a sample holder and a detector. In cathode ray tube the electrons are produced by heating the filament by this the x-rays are generated. These rays are fallen on the powder sample of the material and scattered beam is detected by the detector which gives the diffraction pattern of the sample.

Here, the diffraction pattern was collected by the powder diffractometer 'Bruker AXS D8 Advance' operated at 40 kV and 30 mA within the angular range 5 - 90° (2θ) with graphite monochromator CuK$_\alpha$ at wavelength 1.5406 A° as radiation source.

Figure 2.1: X-ray diffractometer (Bruker AXS, D8 Advance)
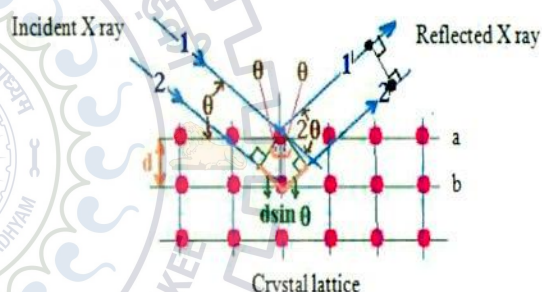
Figure 2.2: A schematic diagram of Bragg's equation

By the 'Scherrer' equation the grain size of crystal can be determined. The 'Scherrer' equation is:

$$dp \rightarrow \frac{0.9\lambda}{B cos\ \theta}$$

Where, d_p is the grain size, λ is the wavelength, B is the width of diffraction peak with radius and θ is the diffraction angle[42].

2.2.2 FIELD EMISSION SCANNING ELECTRON MICROSCOPE (FE-SEM)

A scanning electron microscope is used to produce 3D image of sample by bombarding of high energy electron beam on the surface of the sample. When the electron beam interacts with the atom of the sample it produce signals giving the surface composition, topography and other properties of the sample.

Figure 2.3: Field emission electron micrograph (FEI, Quanta 200F)
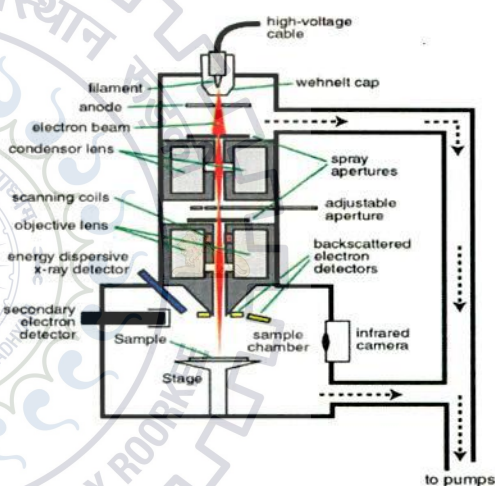
Figure 2.4: A schematic diagram of FE-SEM

In Field Emission Scanning Electron Microscopy (FE-SEM) electrons are emitted via field emission gun upon applying high voltage between a pointed cathode and a anode plate. When an incident electron beam falls on the surface of the sample, the scattered beam contain secondary electrons, backscattered electrons and characteristic X-rays and are detected to create the images. For making the sample conducting the sample is coated by gold. EDAX which is connected to the FE-SEM provides the information about the elemental composition of the sample.

For the present work, the images and elemental composition was collected from the instrument 'FEI Quanta 200F'.

2.2.3 VIBRATING SAMPLE MAGNETOMETER (VSM)

VSM is the technique by which measured the magnetic properties of the samples. In this technique a sample is placed inside the uniform magnetic field to magnetize the sample at different temperature. Then sample is vibrated perpendicularly to the magnetic field typically by using piezoelectric materials. It is simple, versatile and inexpensive, yet permits the precision of magnetic moment measurement in the respect of temperature, crystallographic structure and magnetic field. The sample's magnetic moment is proportional to the induced voltage in the pickup coil. It does not depend on the magnetic strength. In this, the induced voltage is measured by the use of lock-in-amplifier using the piezoelectric signal and gets the hysteresis loop of the sample. This hysteresis loop is used to analyze the nature of magnetic property like ferromagnetic, anti-ferromagnetic, paramagnetic and superparamagnetic[43]. "VSM-155, Princeton applied research" was used for the characterization of samples in the present work.

2.2.4 ATOMIC FORCE MICROSCOPE (AFM):

This technique is used for surface imaging of samples. AFM gives the topographical information of samples by creating an image at the atomic level. There are two modes for operation in AFM; contact mode and non contact mode. The contact mode of operation involves the sideways scanning by the cantilever tip over the surface of the sample. On other hand in non-contact mode the tip-sample separation is increased such that it does not come in contact of the sample. The image of sample is produced by quantifying the force between probe (tip cantilever) and the sample. AFM being non-destructive has the specific advantage that can be used as an imaging tool for the biological samples. High- resolution 3D; x, y and z (normal at the surface)

image can be produced. Its resolution range in x, y-direction is 0.1nm -1.0nm and in z- direction at (at atomic resolution).

AFM consists of cantilever with a sharp tip whose end is used to scan the specimen surface. The tip is made up of silicon or silicon nitride. The tip scans the sample surface by progressively moving backward and forward across the surface. As the tip scan the surface of the sample the force, between the tip and sample varies and this in the force is sensed by the tip connected to a flexible cantilever. The forces between the tip and sample surface lead to a deflection of the cantilever according to Hook's law. The forces that are measured in AFM include the mechanical forces Van der Waal forces, chemical bonding, electrostatic forces and mechanical forces. Typically, the deflection is measured using a laser spot reflected from the top surface of the cantilever towards the position – sensitive photo detector consisting of four sides – by – side photodiode. This laser beam detects the bend occurring in cantilever and calculates the actual position of the cantilever. Thus, AFM records the 3D image of the surface topography of the sample [44].
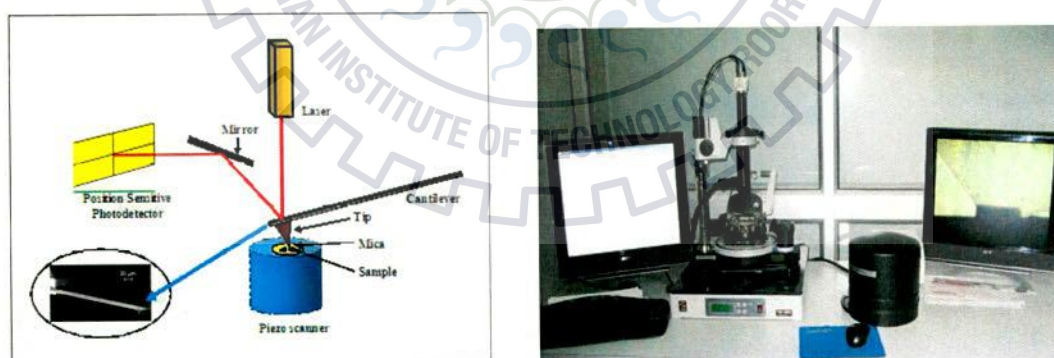
Figure 2.5: a schematic diagram of AFM and used NT- MDT Netgra AFM.

For the present work Atomic force microscopy "NT-MDT Netegra" used i.e. shown in the figure.
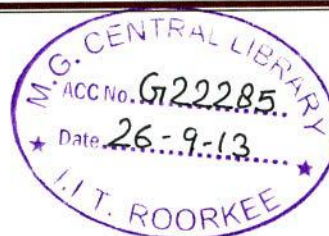
2.2.5   TRANSMISSION ELECTRON MICROSCOPE:

TEM is another microscopic technique used for obtaining 2D image at higher resolution. In this technique an electron beam is transmitted through an ultrafine specimen interacting with specimen or sample and it transmitted through it to produce an image. The image is magnified onto the imaging device such as photographic camera.

Transmission electron microscope uses high energy electron beam (upto < 200 eV accelerating voltage) which are accelerated to nearly speed of light. When an electron beam passes through a thin-section (carbon coated copper grid which contains the sample) of a material, electrons are scattered. An image is recorded by the electromagnetic lenses by focusing of the scattered electrons or a diffraction pattern is obtained depending on the mode of operation. Each of these modes offers a different sight about the specimen. The imaging mode provides a highly magnified view of the micro or nanostructure and in the high resolution imaging mode a direct map of atomic arrangement can be obtained (high resolution EM (HREM)). The electron diffraction pattern presents accurate information about the local crystal structure. For sample preparation a carbon coated cooper grid is used in this technique[45].
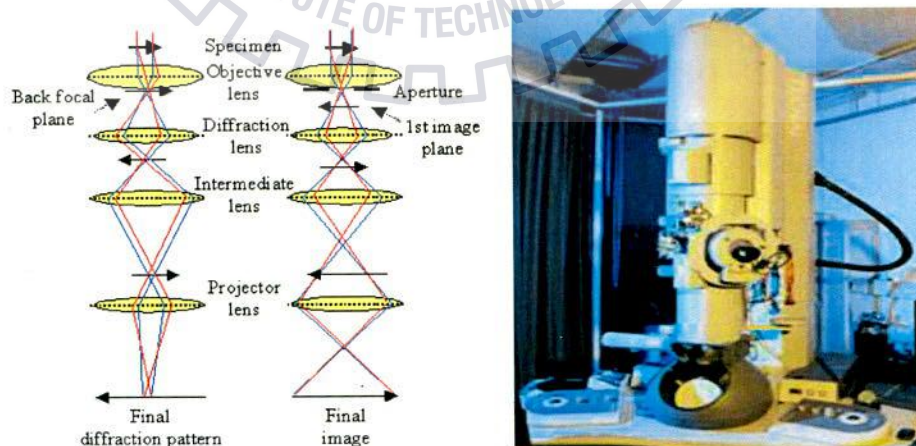
Figure 2.6: a schematic diagram and image of instrument (FEI-TECHNAI 200 keV digital TEM)

2.2.6 UV – VISIBLE SPECTROSCOPY:

UV-Visible spectroscopy refers to absorption or reflectance spectroscopy. Where absorption of electromagnetic radiation by the matter is studies in the domain range from 180 nm to 800 nm. This portion of electromagnetic radiation is designated as UV-visible range. In this technique the concentration of the matter in solution is determined by measuring absorption at some wavelength and applying the Lambert – Beer's law.

The origin of the absorption in this domain is the interaction of the photon from the source and the atom or molecule of the sample. When a molecule absorbs a photon from UV-Vis region the corresponding energy is captured by one of its outer most orbital.

UV-Vis spectrometer, data is collected over the required wavelength range and the spectrum in obtained by plotting the graph between wavelength and transmittance (absorption). The transmittance is the ratio of intensities of incident and transmitted radiation.

$$T = \frac{I}{I_o}$$

And Lambert –Beer's law

$$A = -\ln T = \epsilon.c.l$$

Where   c = concentration

L= length of cubid

ϵ = molar absorptivity

During this period, a number of transition occurred such as σ- σ* > n - σ* > n - Π* > Π-Π* in these transition σ-σ* transition has more energy[46].

Instrument "Shimadzu UV-1800" was used for the UV-Visible analysis of my samples.

2.2.7 FT-IR SPECTROSCOPY:

Infrared spectroscopy, one of the most common spectroscopic techniques for the identification of functional group and bonding between two atoms in the compound. In the near IR and mid IR, the absorption of light by the matter originates from the interaction between the light source and the chemical bond of the sample. If the atoms situated at the two ends of the bond are different, they form a electric dipole that oscillated with a specific frequency. If non-symmetrical bond is irradiated by a monochromatic light source whose frequency is same as the dipole, then the interaction will occur with the bond[47]. The range of infra-red is 2.5μ - 15μ or 4000 to 600cm^{-1}. "Thermonicolet FT-IR NEXUS" instrument was used for FT - IR analysis of my samples.

2.2.8 ATOMIC ABSORPTION MICROSCOPE:

Atomic absorption spectroscopy is a technique used for determining the concentration of a particular metal element in a sample. This technique is used to analyze the concentration of over 70 different metals in the solution.
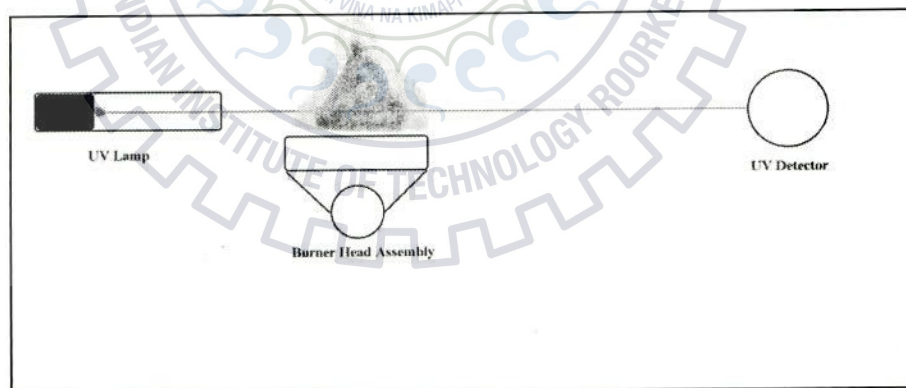
This technique is based on the absorption spectroscopy which assesses the concentration of analyte in a sample that relies on Beer-Lamberts law. In brief, the electrons on atoms in the atomizer can be promoted to higher orbital for a short amount of time by absorbing a set of

quantity of energy. This amount of energy (wavelength) is specific to a particular electron transition in a particular element, i.e. each wavelength corresponds to only one element. This gives the technique its chemical selectivity. Thus it is possible from Beer-Lambert law to calculate how many of these transitions took place and thus get a signal that is proportional to the concentration of the element being measured. But on applying the Beer-Lambert law directly in AAS is difficult due to variations in atomization efficiency from the sample matrix and non uniformity of concentration and path length of analyte atoms, thus concentration measurement are usually determined from a working curve after calibrating the instrument with standard of known concentration[48]. "Perkin Elmer AAnalyst 800" model was used for the concentration measurement.

2.3 Methods

Preparation of magnetite nanoparticles:

Magnetite nanoparticles were prepared by co-precipitation process with minor modification, in this process magnetite nanoparticles were prepared by dissolving anhydrous ferric chloride (2 mol dm^{-3}) and ferrous sulfate heptahydrates (1 mol dm^{-3}) with the molar ratio of 2:1 in the nitrogen environment with vigorous stirring. This reaction was preceded in nitrogen environment to avoid any oxidation during reaction period. After completion of the reaction add sodium hydroxide (1 mol dm^{-3}) drop wise in the solution to make it alkaline. Stir the solution again and get the black precipitate of Fe_3O_4 and dried under vacuum at 60°C.

Cysteine coated ferrite nanoparticles synthesis:

Magnetite Nanoparticles (0.2 g) were dispersed in distilled water. To this solution, aqueous solution of cysteine conataing equivalent to magnetite was added. The resulting suspension was stirred for 24 h, it produces the cysteine coated nanoparticles[49].

Adsorption studies:

For adsorption studies, a 100 ppm solution of $Pb(NO_3)_2$, pH 6.0 was prepared by using acetate buffer (0.2 mol dm^{-3}) and was used as a stock solution. The adsorption studies were performed by mixing 5 mg magnetite nanoparticles with 10 ml $Pb(NO_3)_2$ solution at varying concentrations (5, 10, 15, 20, 25 and 30 ppm). This experiment were performed with 10 ml of 10 mg/L with 5 mg cysteine coated nanoparticles at different pH (2-10) to obtain optimum pH at which maximum adsorption occurs. Perchloric acid and NaOH were used for pH adjustment. Adsorption isotherm studies were performed by varying the initial concentration from 5 to 30 ppm at different temperature. For equilibration time, the cysteine coated Nanoparticles were shaken at mechanical shaker for different time (in h) and found that after 3 hr there reaches a saturation point for absorption. This study was carried out at different time. Adsorption isotherm measurements were made at different temperature (K) 308, 313 and 318.

2.4 Characterization Techniques

2.4.1 Sample preparation for XRD measurement:

The powder sample was directly used for powder X-ray analysis.

2.4.2 Sample preparation for VSM studies:

For VSM studies, a known amount of powder sample was vibrated between two magnets at appropriate 10 tesla magnetic field and magnetic moment of the sample was measured and used to obtain the hysteresis loop.

2.4.3 Sample preparation for FE-SEM:

One drop of the diluted sample was placed on a glass slide and this glass slide was stuck on the stub by the help of carbon tap. The gold coating was done by sputtering of gold for making the non-conducting sample to conducting and this stub was placed in the instrument for further characterization.

2.4.4 Sample preparation of AFM studies:

One drop of diluted sample was placed on a glass slide and dried it at room temperature in dark. This glass slide was used directly for measurement.

2.4.5 Sample preparation for zeta sizer:

Sample was dispersed in distilled water by sonication. The dispersed solution for the further analysis by zetasizer.

2.4.6 Sample preparation for FT-IR measurement:

A pinch of sample with KBr powder was mixed in a mortar and used to prepare a KBr pellet using a hydraulic press which was used for the FT-IR measurement.

2.4.7 Sample preparation for thermal analysis:

A certain amount of sample was placed in the alumina crucible of the instrument.

2.4.8 Sample preparation for TEM analysis:

For TEM analysis the 300 times diluted sample was applied on the carbon coated copper grid and dried at room temperature. This grid was placed in TEM holder and the SAED pattern , particle size and morphology of the sample were studied.

2.4.9 Sample preparation for UV-Visible:

The liquid sample was placed in 1 cm cuvette and UV-visible spectra in the 200-800 nm range were collected.

2.4.10 Sample preparation for AAS:

The solution decanted from the cysteine coated magnetite was used for the AAS analysis.

Adsorption

Adsorption is a physical as well as chemical phenomenon. Chemical process involves the interaction between surface atom of adsorbent and atom of adsorbate. This type of adsorption is called **chemisorption**. It is adhesion of atom, ions and molecule form the solid, liquid and gas to the surface. Adsorption is a surface based phenomenon while adsorption is applied for whole volume. Adsorption normally described in isotherm which is the amount of adsorbate on the surface of adsorbent as the function of its pressure or concentration. Different types of adsorption isotherm are given below:
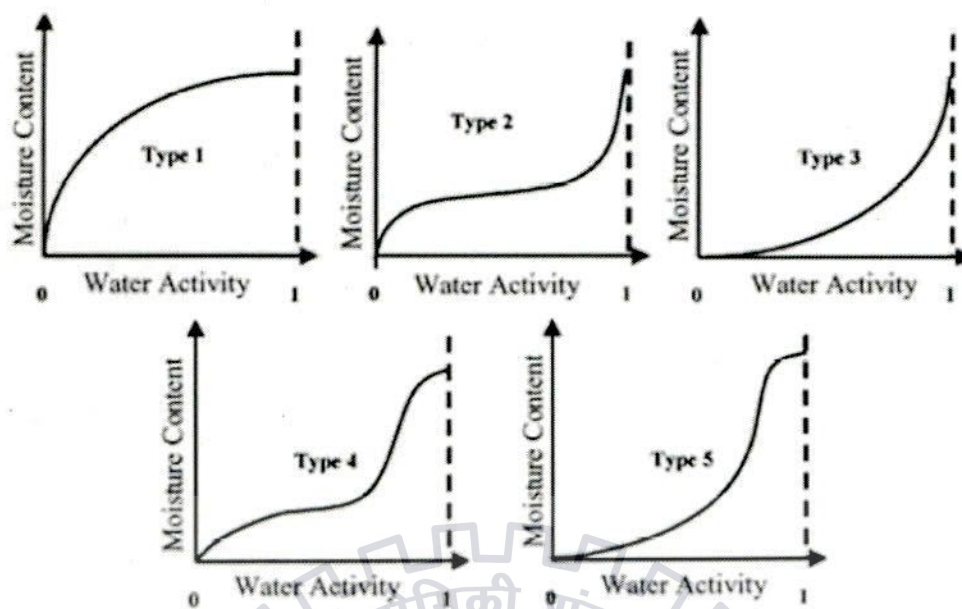
Figure 2.7: Types of Adsorption

Adsorption studies involve measuring of the extent of adsorption as a function of concentration or pressure. Different isotherms popularly used are:

1. Freundlich isotherm

2. Langmuir isotherm

3. BET isotherm

1. Freundlich isotherm:

For adsorption from solution, a commonly used isotherm is the freundlich adsorption isotherm. If x is the mass of the solute adsorbed on mass m of adsorbent and c is the concentration of the solute in the solution, then the Freundlich isotherm is represented by:

$$x/m = k\,c^n$$

Where, k and n are empirical constant which depends on the nature of the solute and nature of the adsorbent. Taking logarithm of both the side in above equation:

$$\ln x/m = \ln k + n \ln c$$

If the plot between $\ln x/m$ and $\ln c$ comes out to be a straight line it suggests the adsorption follows Freundlich isotherm. The above two isotherm are restricted to the formation of monomolecular layer on the surface of adsorbent.

Langmuir isotherm:

Langmuir isotherm is describing adsorbate adsorbed on the surface of the adsorbent. It depends on three assumptions:

- The surface of the adsorbate is in contact in the solution with the adsorbent.
- The surface contains the active sites for adsorption.
- It is monolayer adsorption.

Langmuir adsorption isotherm is represented by the equation:

$$\phi = \frac{KC}{1+KC}$$

Where, dividing the numerator and denominator by K and making use of the fact that q will be proportional to ϕ and the useful form of the equation is

$$q = \frac{q_m K_a C}{1+K_a C}$$

Where, q_m = q for a complete monolayer

K_a = a coefficient

$$\frac{1}{q_m} = \frac{1 + K_a C}{q_m K_a C}$$

$$\frac{1}{q} = \frac{1}{q_m K_a C} + \frac{1}{q_m}$$

If the slope of this equation is $1 / q_m K_a$, a plot of $\frac{1}{q}$ versus $\frac{1}{C}$ should give a straight line it suggests

the adsorption follows Langmuir equation of slope $1 / q_m K_a$ and an intercept to be $1/ q_m$.

BET adsorption isotherm:

In case the process of adsorption leads to the formation of multi-layers, such isotherms are derived by Brunauer, Emmett and Teller. BET isotherm has been applied in gas adsorption, porous steam in surfaces and solids as well as in water by homogenous polymers[50].
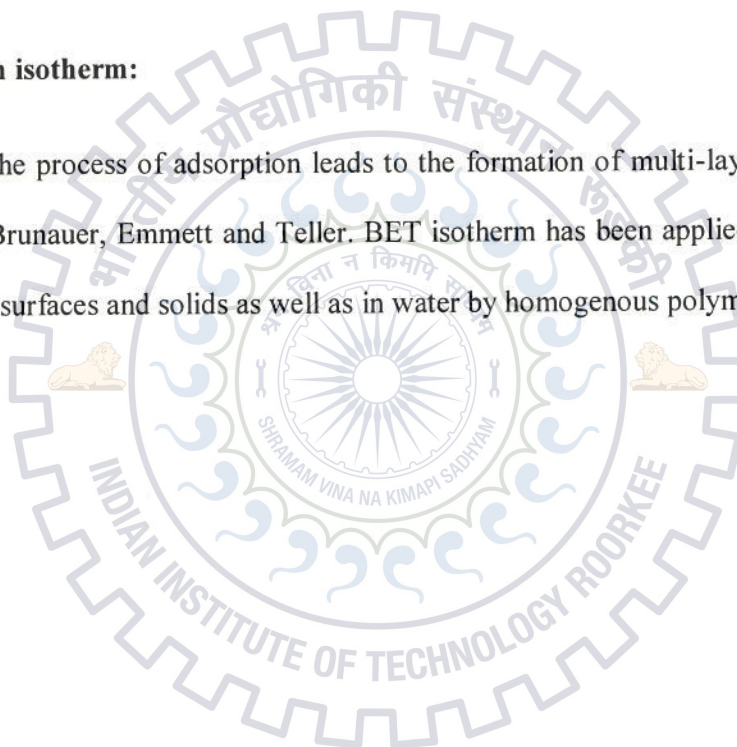
CHAPTER - 3

RESULT AND DISCUSSION

3.1 *XRD pattern of coated and non-coated Fe₃O₄ nanoparticles:*

Figure 3.1, shows XRD patterns of as prepared Fe_3O_4 and cysteine coated - Fe_3O_4 nanoparticles. In XRD pattern each of these samples six characteristic peaks have been marked. These peaks matched with characteristic peaks due to magnetite having the inverse spinel structure (JCPDS card no. 85-1436). The crystalline size of cysteine coated - Fe_3O_4 and Fe_3O_4 nanoparticles calculated by the Debye - Scherrer formula comes out to be 10.2 nm and 12.1 nm respectively.
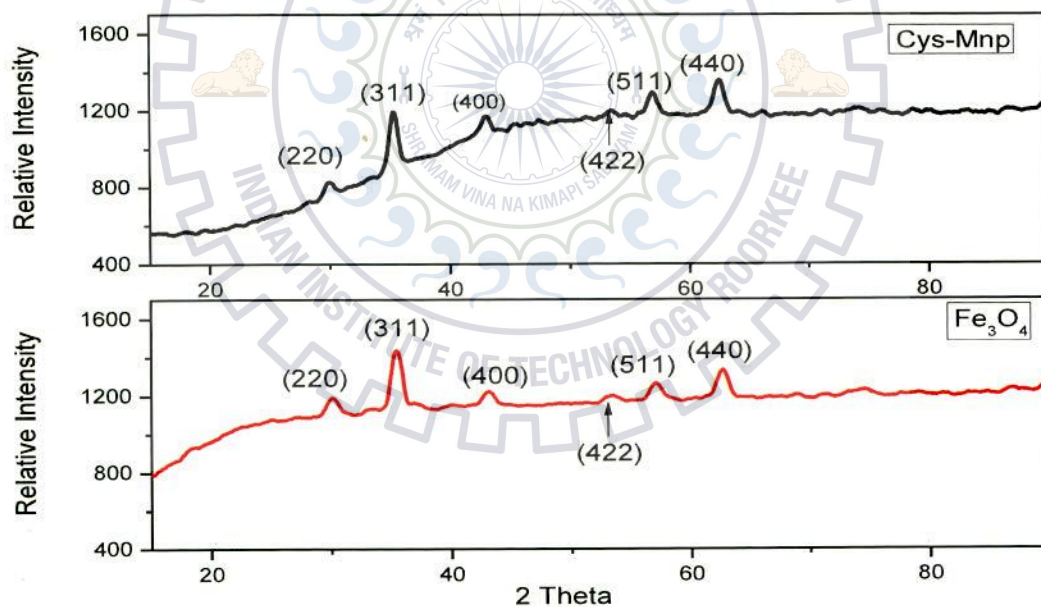
Figure 3.1: XRD patterns of Fe_3O_4 and Cysteine coated - Fe_3O_4 nanoparticles

3.3   *Characterization by FE-SEM:*

Figure 3.2 and 3.3 shows the SEM micrograph of Fe_3O_4 and cysteine coated - Fe_3O_4

nanoparticles and these micrographs shows that the morphology of particles is spherical.
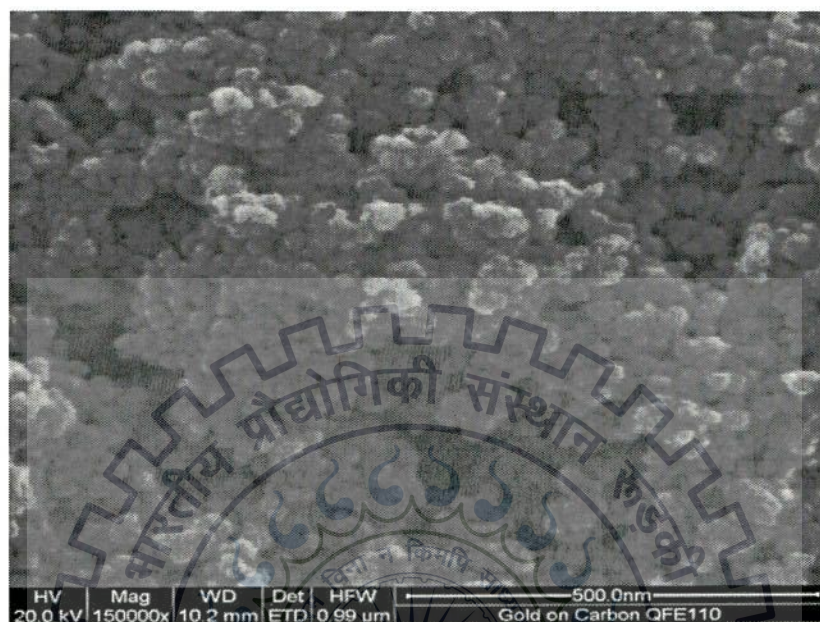
Figure 3.2: SEM micrograph of Fe_3O_4 nanoparticles.
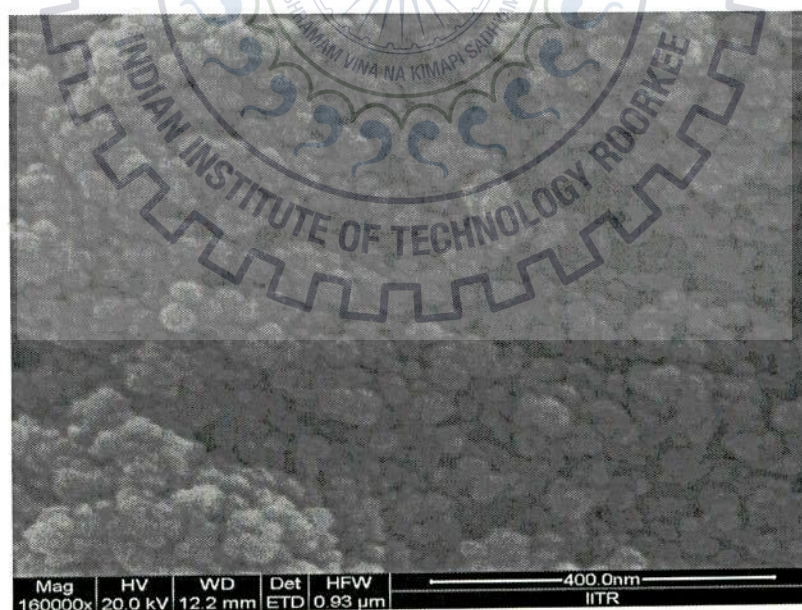
Figure 3.3: SEM image of Cysteine coated - Fe_3O_4 nanoparticles.

(a)   (a')
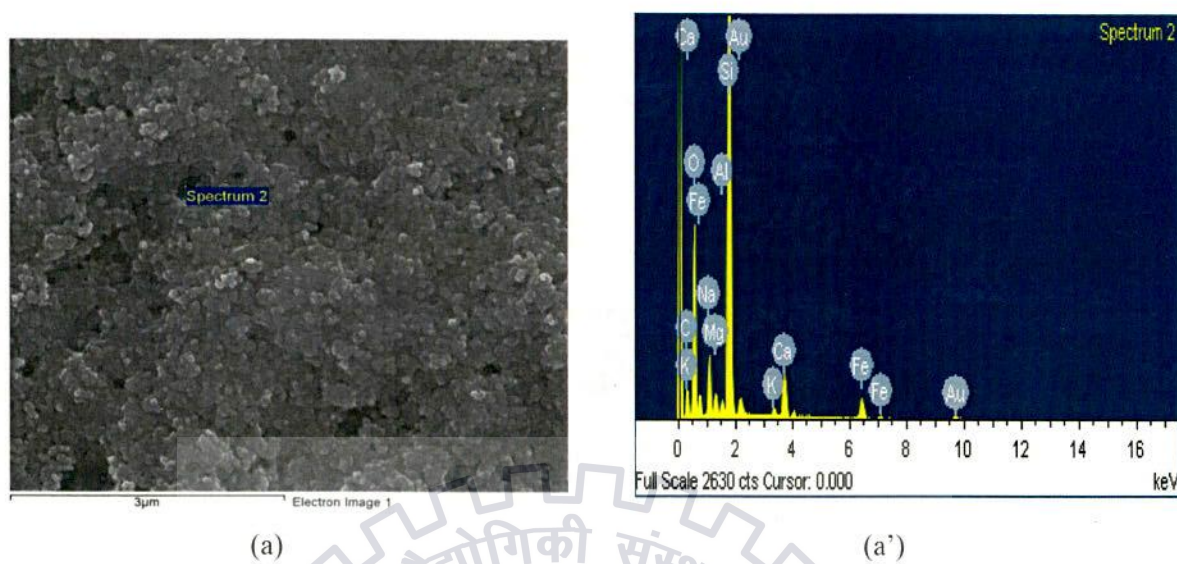
Figure 3.4 (a and a'): SEM-EDAX of Fe_3O_4 nanoparticles.

EDAX of Fe_3O_4 and cysteine coated - Fe_3O_4 nanoparticles as shown in the images (a and b) were used to find the chemical composition of these nanoparticles.

(b)   (b')
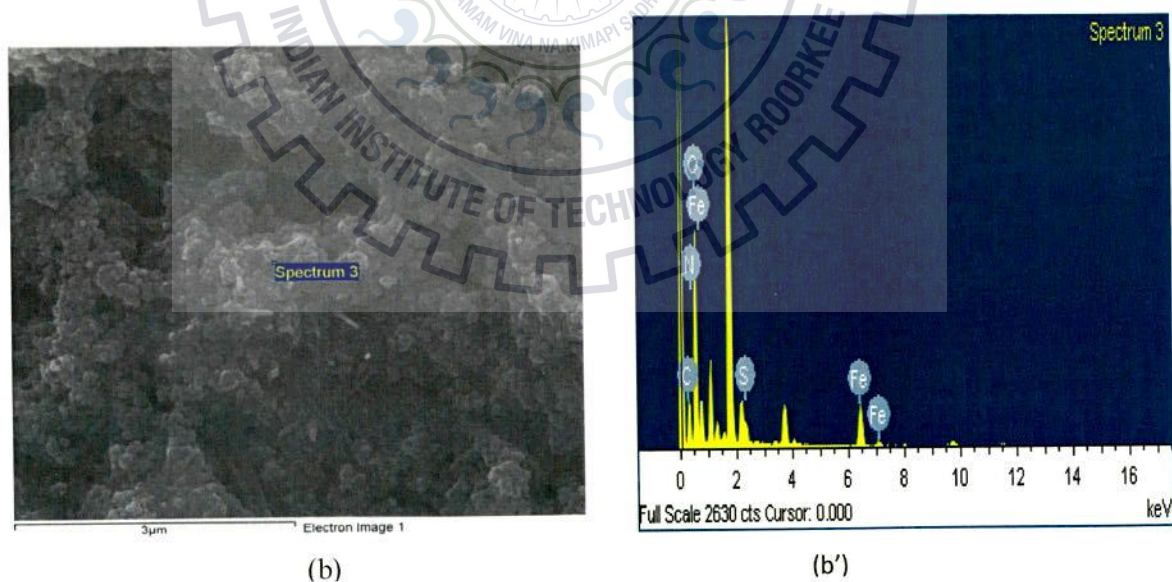
Figure 3.5 (b and b'): SEM-EDAX of cysteine coated - Fe_3O_4 nanoaprticles.

EDAX analysis of cysteine coated - Fe_3O_4 carried out for different particles in the above shown images show the presence of Fe, C, N, S and O suggesting the coating of Fe_3O_4 by cysteine.

3.3 *Characterization by TEM:*
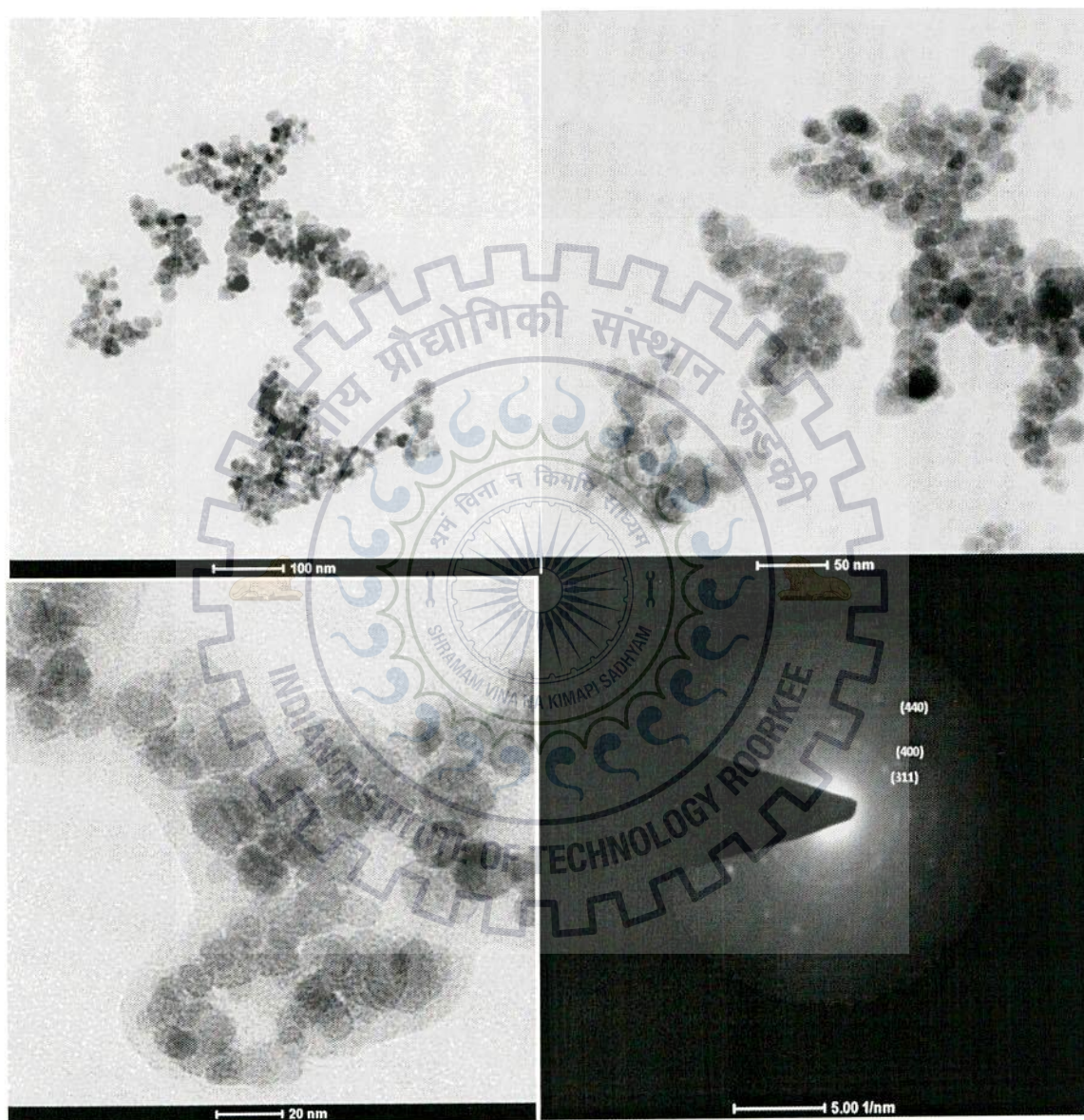
Figure 3.6: TEM images at 100nm, 50nm and 20nm and SAED pattern of Cysteine coated - Fe_3O_4 nanoparticles.
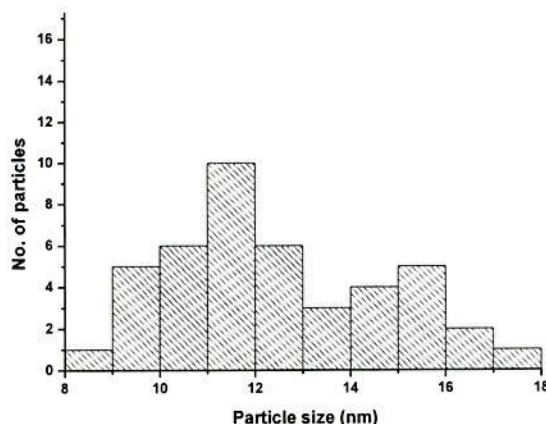
Figure 3.6 (a): The histogram of Cysteine coated – Fe_3O_4 nanoparticles.

TEM images of cysteine coated – Fe_3O_4 nanoparticle are shown in the figure. 3.6 and 3.6 (a). These images reveal the formation of aggregated chains of spherical nanoparticles in which the Fe_3O_4 present in core is surrounded by cysteine. From these micrographs the average diameter (size distribution) of the cysteine coated nanoparticles is estimated to be 12 nm. The SAED pattern of cysteine coated - Fe_3O_4 nanoparticles shows a set of rings masked with some spots. Indexing of SAED pattern of cysteine coated - Fe_3O_4 shows the diffraction from (311), (400) and (440) planes, which match to those of Fe_3O_4 phase identified in XRD.

3.4 *AFM analysis:*

2D and 3D AFM images along with the size histogram of Fe_3O_4 and cysteine coated - Fe_3O_4 nanoparticles are given in figure 3.7 and 3.8 shows their morphology spherical but these particles are agglomerated possibly due to their high magnetization. From the 2D image, cysteine coated particles comes out to be 69.7 nm which is about 7 times higher to that of uncoated particles (average size 10 nm) due to agglomeration. The roughness of coated and non-coated Fe_3O_4 nanoparticles is observed to be 13.316 nm and 2.285 nm respectively.
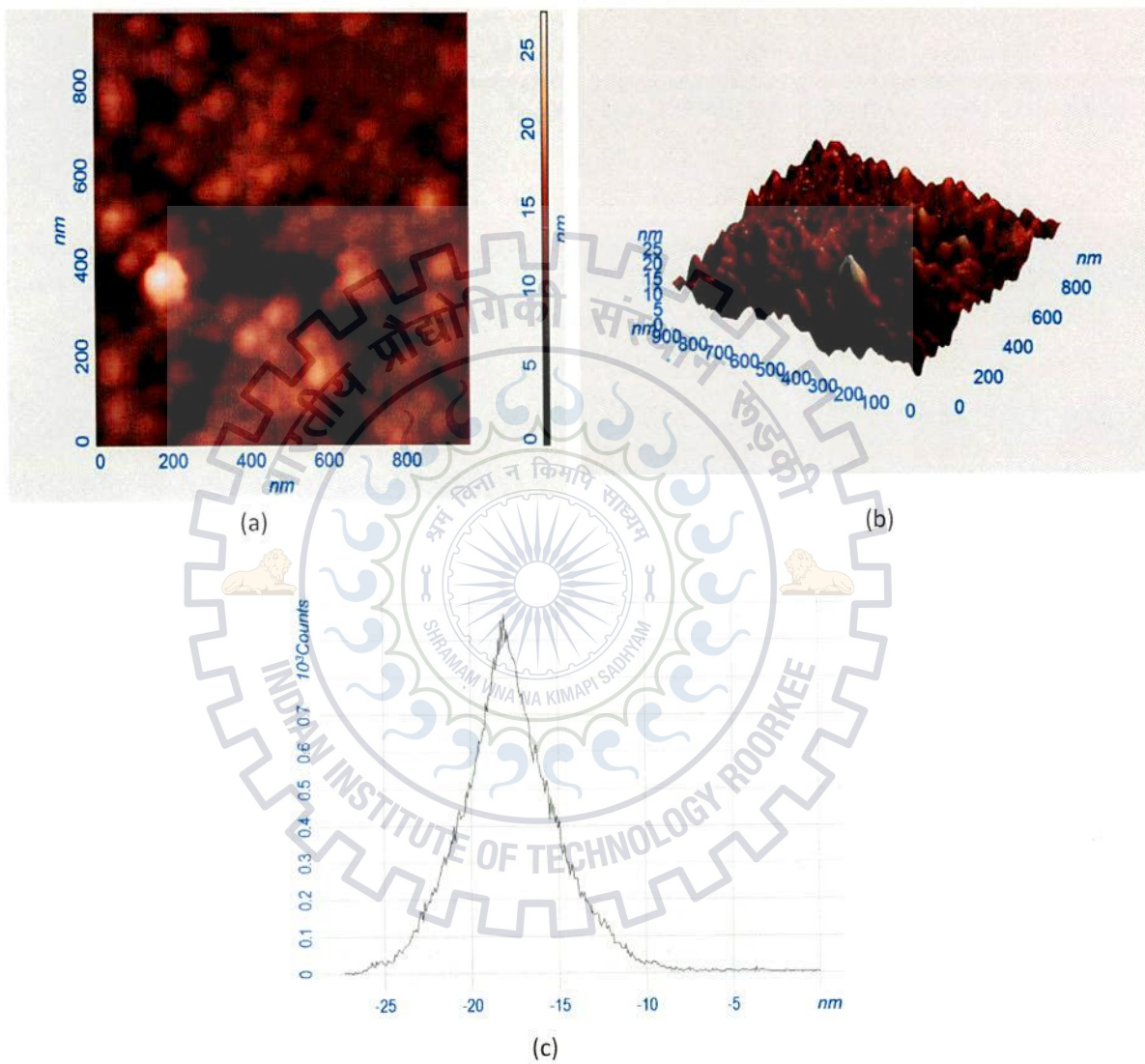
Figure 3.7: (a) and (b) are the AFM images and and (c) is the histogram of Fe_3O_4 nanoparticles.

(a)

(b)

(c)
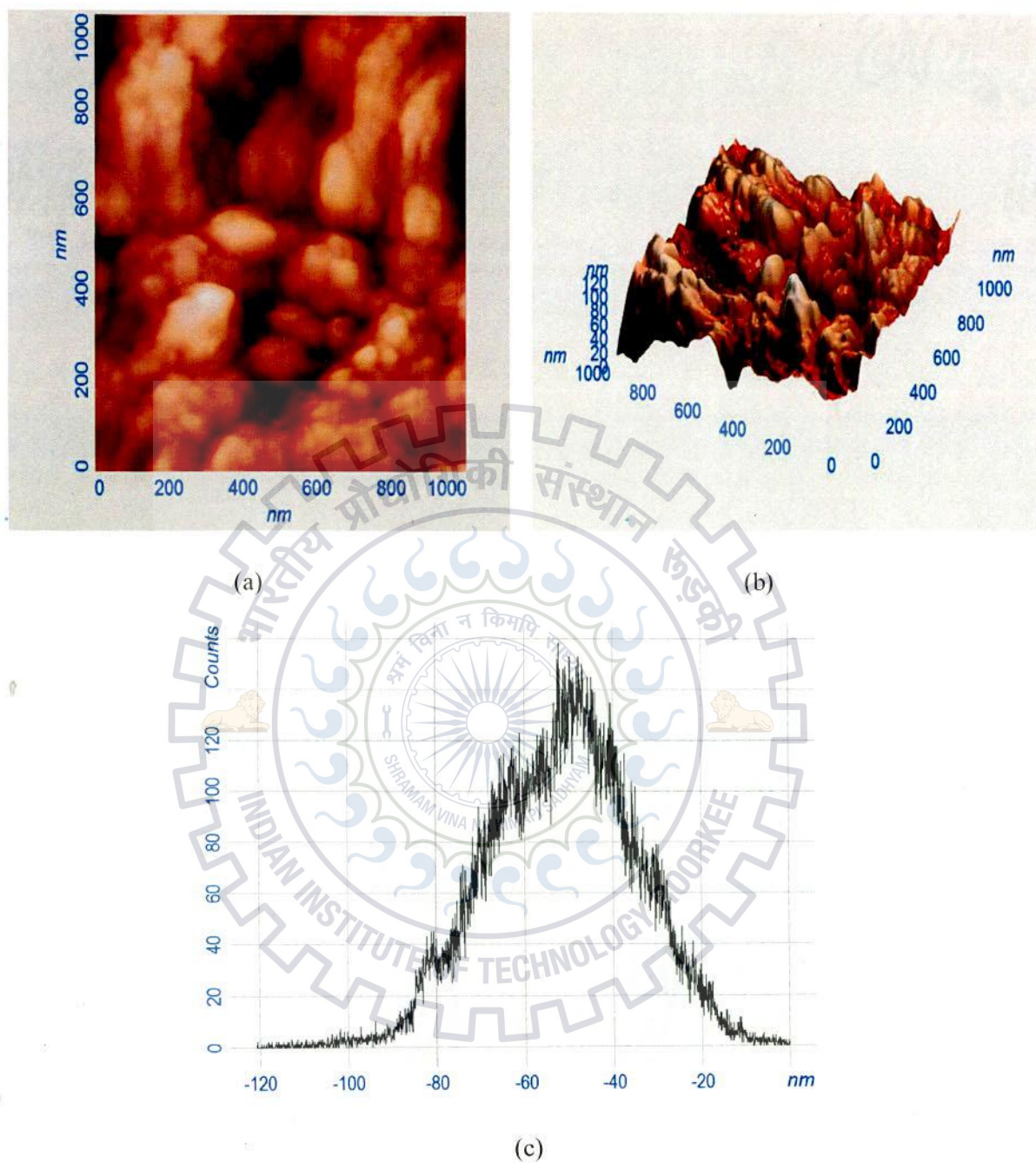
Figure 3.8: (a) and (b) are the AFM images and (c) is the size histogram of Cysteine coated -

Fe_3O_4 nanoparticles.

3.5 *Characterization by Zeta sizer:*

Using zeta probe, the size distribution and the zeta potential were measured and are given in figure 3.9 (a) and (b) respectively. From figure 3.9 (a) the hydrodynamic radius of cysteine coates - Fe_3O_4 nanoparticles was found to 69.85 nm by the distribution of intensity and figure 3.9 (b) the zeta – potential of cysteine coated - Fe_3O_4 nanoparticles is -34.5 mV. This value shows the nanoparticles are fairly stable and carry negative charge.

(a)   (b)
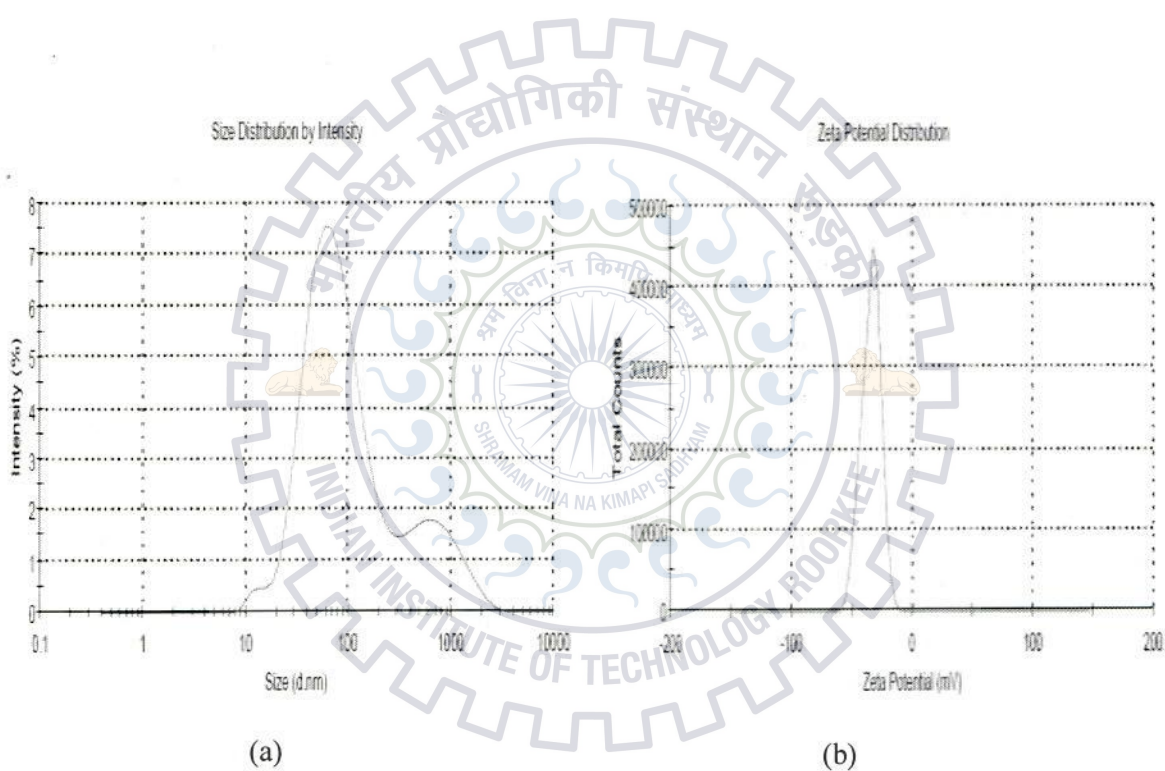
Figure 3.9: (a) and (b) are represent the zeta size and zeta potential of Cysteine coated - Fe_3O_4 nanoparticles.

3.6 FT-IR Studies of Fe_3O_4, pure cysteine and cysteine coated - Fe_3O_4 nanoparticles:

Figure 3.10 (a): FT-IR Spectra of Fe_3O_4 nanoparticles.
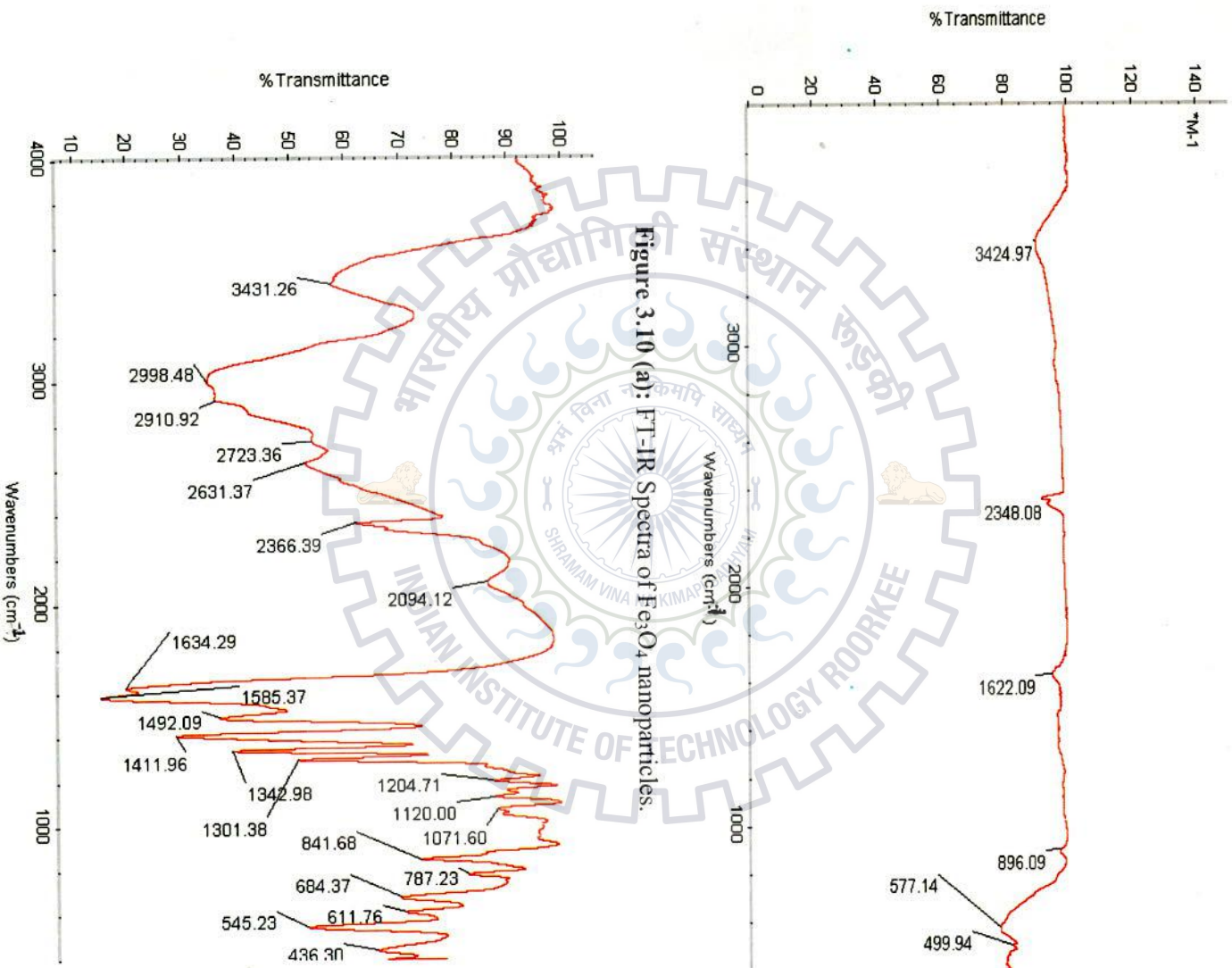
Figure 3.10 (b): FT-IR spectra of pure cysteine
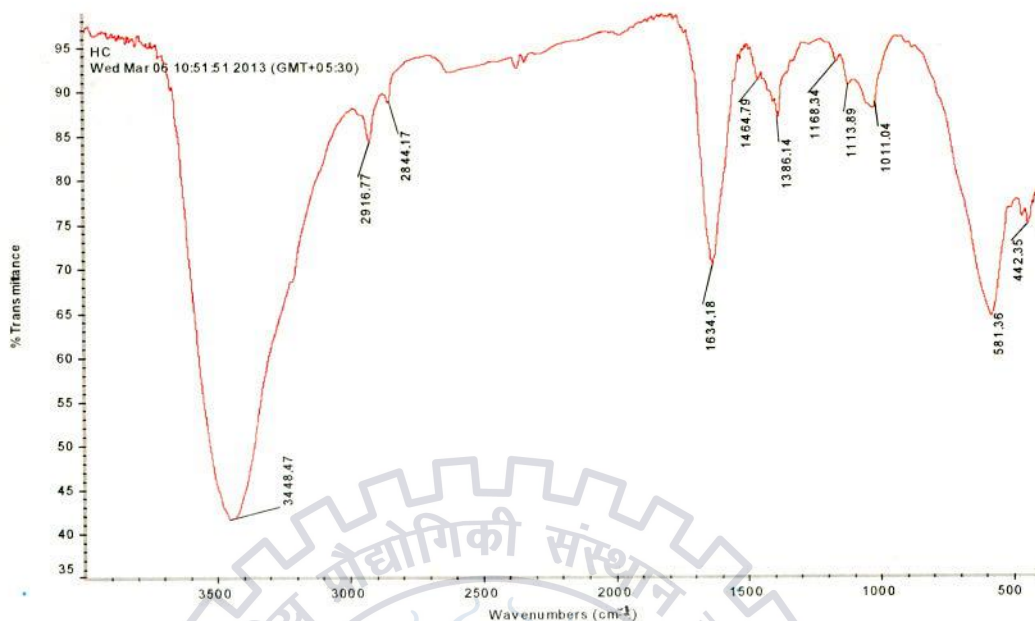
Figure 3.10 (c): FT-IR spectra of Cysteine coated - Fe_3O_4 nanoparticles.

Functional group	Frequency (cm^{-1})		
	Fe_3O_4	Pure Cysteine	Cysteine coated - Fe_3O_4
NH_3^+ str.	----	3431	3448
S-H str.	----	2631	-------------
NH_3^+ deg.deform	----	1634	1634
COO^- asy. str	----	1585	----------
NH_3^+ sym. deform	----	1492	1464
COO^- sym. str.	----	1411	1386
C-N, C-C str.	----	1071	1113
S-H bending	----	841	--------------
Fe-O str.	577	.....	581

Table 1: Shows the peak position of Fe_3O_4, pure cysteine and Cysteine coated - Fe_3O_4

nanoparticles.

FT-IR spectra of bare Fe_3O_4, pure cysteine and cysteine coated - Fe_3O_4 are shown in figure 3.10 (a), (b) and (c). The respected spectral data are given in the table. An examination of IR reveal that the peak due to different functional group of cysteine specifically NH_3^+ str. NH_3^+ deform and NH_3^+ sym.deform peak get influenced and the peak due to S-H str., COO- asy. str and S-H bending are completely vanished suggesting an interaction of Fe_3O_4 through these groups. The peak due to C-N, C-C str. is also most to higher wave number. Besides, Fe-O str. which in the absence of cysteine gives a peak at 577 cm^{-1} also get shifted to higher wave number at 581 cm^{-1} in the presence of cysteine. These observations clearly suggest that coating of cysteine is affectively bonded to Fe_3O_4.

3.7 *UV-Visible Spectra of pure Cysteine, Cysteine coated - Fe_3O_4 and Fe_3O_4 nanoparticles:*
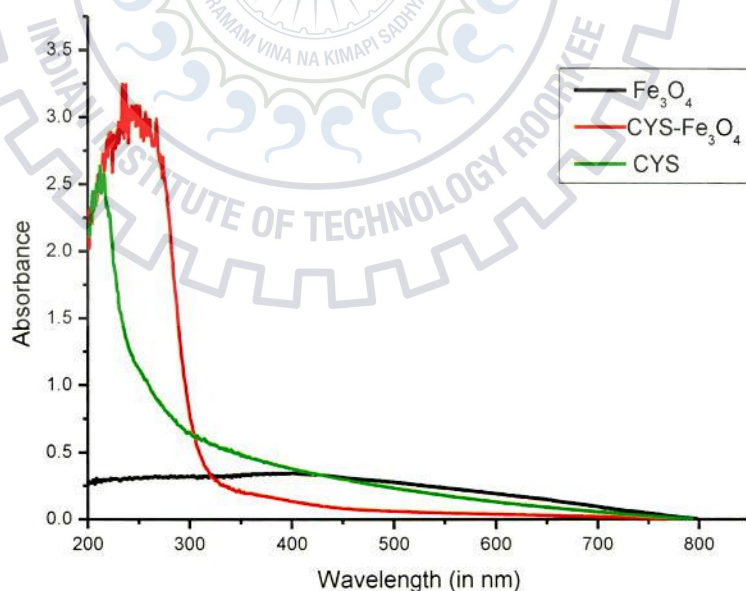
Figure 3.11: Shows the UV-Visible spectra of Fe_3O_4, Cysteine coated - Fe_3O_4 and Cysteine.

The figure 3.11 shows the optical absorption spectra of pure cysteine, Fe_3O_4 and cysteine coated - Fe_3O_4 nanoparticles. UV-Visible spectra of aqueous cysteine show a peak at 214 nm which shifts towards higher wavelength for cysteine coated - Fe_3O_4 nanoparticles and appear at 244nm. This change also suggests an interaction between cysteine and Fe_3O_4 nanoparticles.

3.8 *Thermal Studies of Fe_3O_4 and Cysteine coated - Fe_3O_4 nanoparticles:*
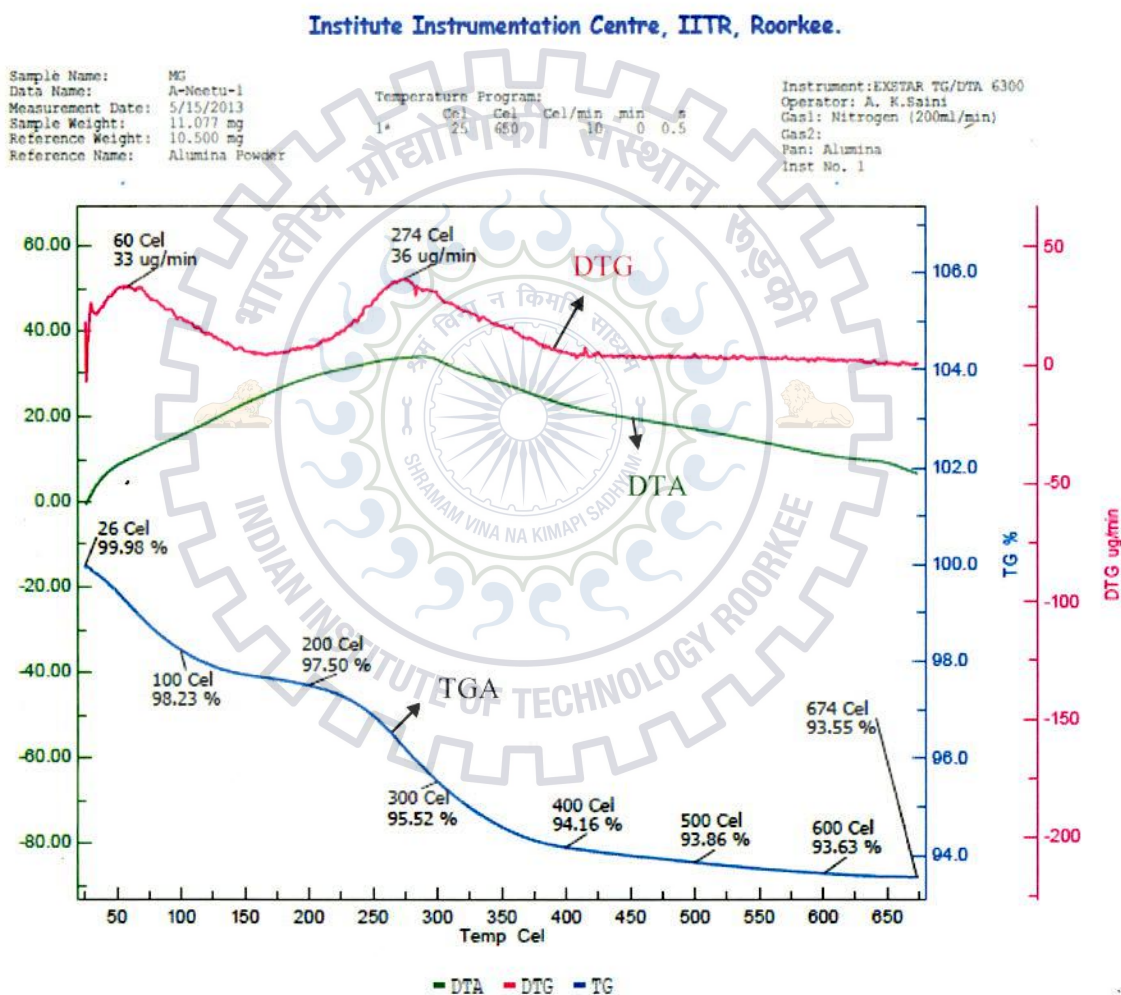
Figure 3.12 (a): TGA-DTA-DTG plot of Fe_3O_4 nanoparticles.

TGA-DTA-DTG curve of Fe_3O_4 nanoparticles under nitrogen environment is shown in figure 3.12 (a). The thermal analysis of Fe_3O_4 nanoparticles was carried out in the temperature range

from 25 to 650°C at the heating rate 10°C/min. In TGA curve of Fe_3O_4 nanoparticles the first mass loss is about 60°C and percent loss is about 1.75% which is probably due to the removal of surface hydroxyl groups and second mass loss occurred at 274°C, the percent mass loss is about 4.46% from start, which is due to the phase transition from Fe_3O_4 to FeO. From 274 °C to 500 °C the percent mass loss is about 1.66 %. At this temperature there exists FeO phase. DTA curve shows that these nanoparticles undergo exothermic reaction upon heating.
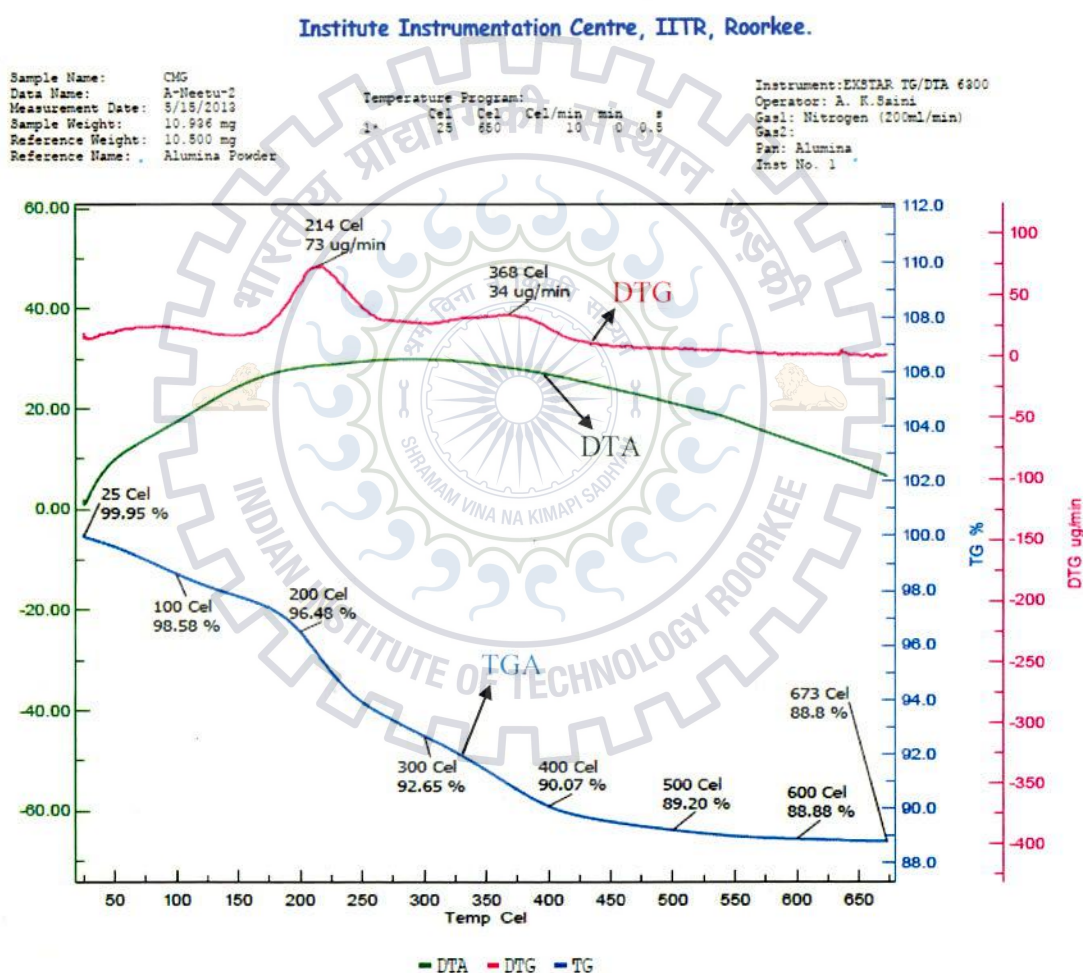
Figure 3.12 (b): TGA-DTA-DTG plot of Cysteine coated - Fe_3O_4 nanoparticles

A typical TGA-DTA -DTG curve under nitrogen environment shown in the figure 3.12 (b) for cysteine coated - Fe_3O_4 nanoparticles. Thermal analysis was carried out in the temperature range

from 25 - 650 °C at the heating rate 10 °C/min. In this TGA curve of cysteine coated - Fe_3O_4 shows the three measure percent mass loss, first percent mass loss at 100 °C is about 1.37 % which is due to the removal of surface amino groups. Second, mass loss is at 214 °C is about 5.93% from 100 °C which is approximately the boiling or decomposition temperature of cysteine (201 – 300 °C), and third percent mass loss start at about 400 °C, it is about 2.58% which can be assigned to the decomposition of Fe_3O_4 into FeO. Here, also DTA curve shows the exothermic reaction upon heating. These observations show the thermal – stability of cysteine coated - Fe_3O_4 is increased after coating.

3.9   *VSM Studies of the Synthesized Nanoparticles:*

VSM curves of Fe_3O_4 and cysteine coated - Fe_3O_4 nanoparticles at room temperature are shown in figure 3.13. These curves reveal that the superparamagnetic behavior of both the samples. From these curves, the magnetic moment of Fe_3O_4 and cysteine coated – Fe_3O_4 nanoparticles were found to be 74.1 emu/g and 66.8 emu/g respectively.
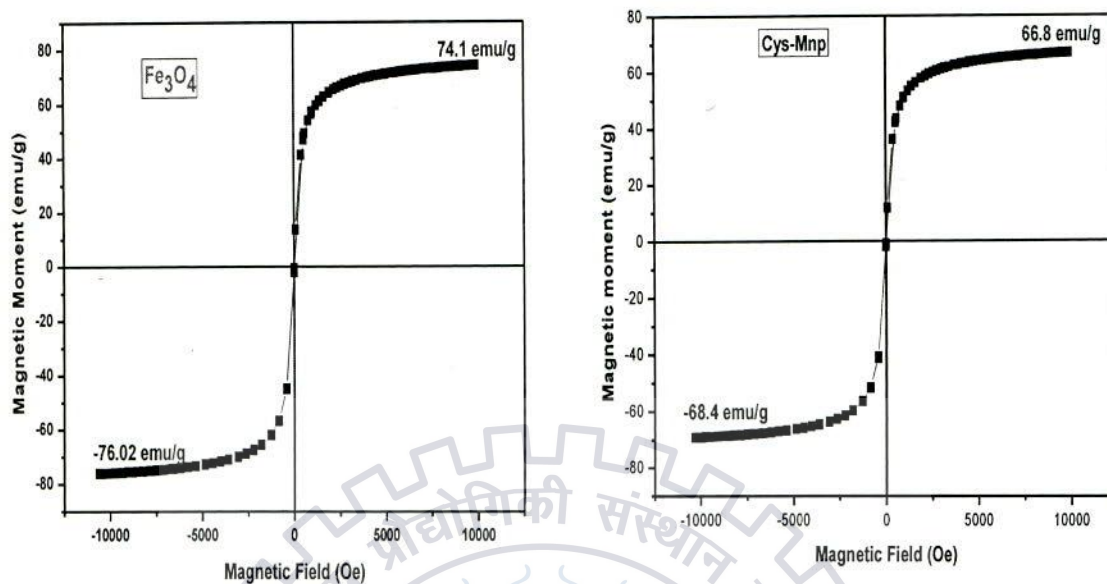
Figure 3.13: VSM curves of Fe_3O_4 and Cysteine coated - Fe_3O_4 nanoparticles

3.10 *Adsorption Studies:*

To explore the sorption capacity of the cysteine coated - Fe_3O_4 nanoparticles, batch adsorption experiments for the removal of Pb^{+2} ions from the aqueous solution were carried out at ambient temperature. In order to optimize the adsorption efficiency of cysteine coated - Fe_3O_4 nanoparticles, the effect of time and pH on the adsorption efficiency were analyzed.

Effect of pH:

Adsorption efficiency of lead on cysteine coated – Fe_3O_4 nanoparticles was examined over a pH range of 2-10 and the data of these measurements are summarized in Table – 2

pH	Before adsorption concentration (ppm)	Concentration of lead after adsorption (ppm)	Adsorption efficiency (%)
2	10.02	9.09	9.3
4	8.352	2.792	66.5
6	6.642	0.242	96.3
8	2.182	0.417	80.88
10	6.793	0.675	90.06

Table 2: Lead removal efficiency by cysteine coated - Fe_3O_4 nanoparticles at different pH.

From the above data it is seen that the extent of adsorption of Pb^{+2} is increased from pH 2-6 and thereafter it is decreased up to pH 8.0. These changes are depicted graphically in figure 3.14.

Figure 3.14: Effect of pH on lead removal efficiency by Cysteine coated - Fe_3O_4 nanoparticles $(0.5gL^{-1})$ concentration 10 ppm and temperature 35°C.

The lead removal efficiency at pH 6.0 – 8.0 increases as compared to that of lower pH. The experimental highest adsorption efficiency is obtained at pH 6.0. So, further experiment was done at optimum pH 6.0 with 10 ppm lead concentration.

Optimization of time of equilibration:

The time of equilibration was optimized by varying the time period for which the sample was equilibrated by shaking the sample on a mechanical shaker. Adsorption data of these experiments are summarized in Table – 3 and its plot is given in figure – 3.15.

Serial no.	Time (h)	Concentration of lead after adsorption (ppm)	Amount adsorbed (ppm)
1.	0	10.00	0
2.	0.25	4.90	5.09
3.	0.5	3.95	6.04
4.	1.0	2.32	7.67
5.	1.5	2.25	7.74
6.	2.0	1.77	8.22
7.	2.5	1.80	8.19
8.	3.0	1.53	8.46

Table 3: Lead removal efficiency at different time.

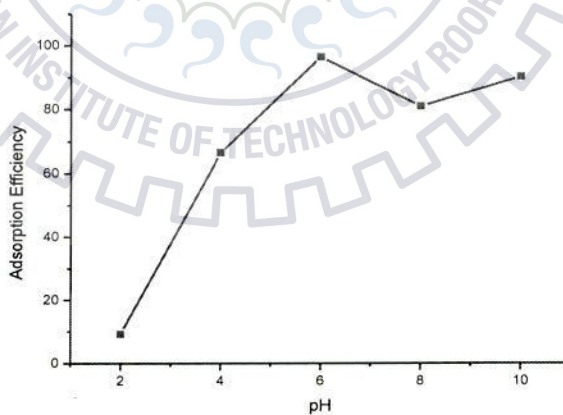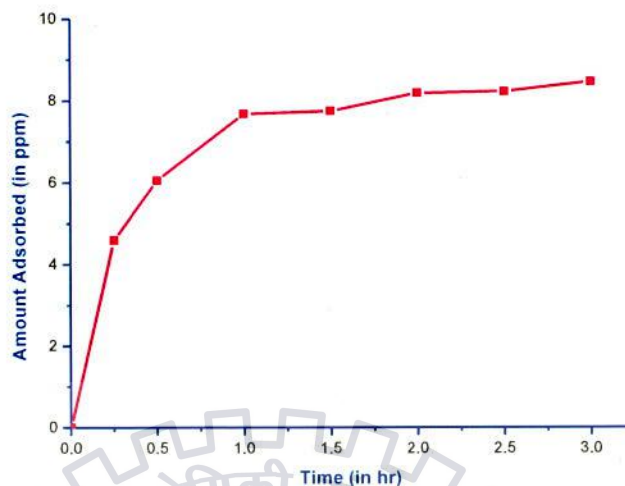**Figure 3.15:** Effect of time variation (in hr) on lead removal efficiency by Cysteine coated - Fe_3O_4 nanoparticles $0.5gL^{-1}$ at lead concentration 10 ppm, and temperature 35^oC.

These experiments demonstrate that this system attain the plateau value after about 1 h of equilibration.

The adsorption data at equilibrium for a wide range of adsorbate concentration are well defined by various adsorption isotherms. The adsorption data at equilibrium for a wide range of adsorbate concentration are well defined by various adsorption isotherms. The adsorption isotherm in the present case is shown in figure – 3.16. The observed curves show that the adsorption of Pb^{+2} on cysteine coated - Fe_3O_4 follows Type – I behavior. To further investigate the adsorption behavior, adsorption isotherm were measured at different temperatures (308–318 K). Adsorption isotherms obtained at three temperatures are shown in figure 3.16.
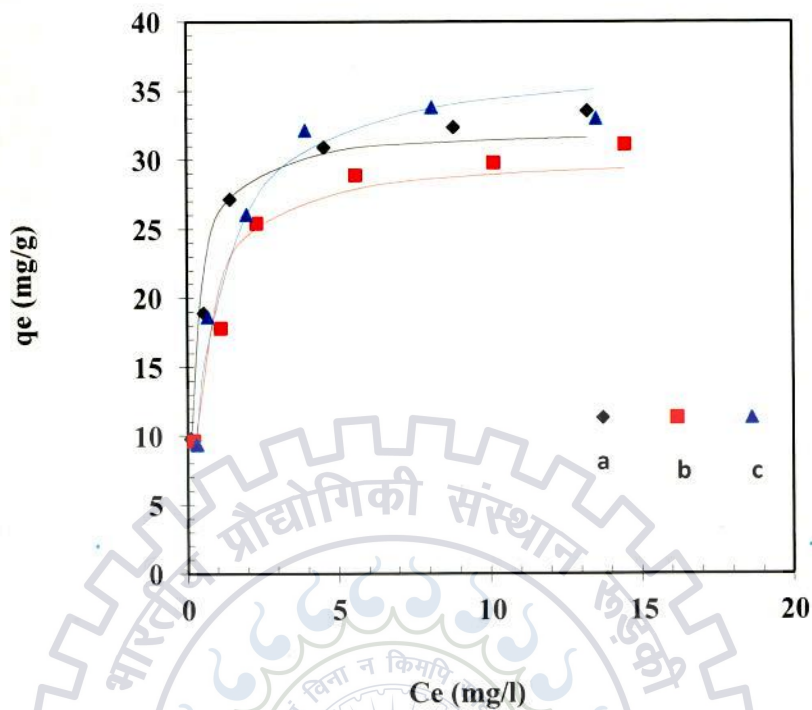
Figure 3.16: Langmuir adsorption isotherm fitting graph of a) at 308K, b) 313K, c) 318 K.

The Langmuir constants obtained from these curves are summarized in Table – 4. For all these plots the value of R^2 or correlation coefficient is < 0.97. Moreover, the R^2 values of Langmuir isotherm are greater than other isotherm, that means these data found to best fit in Langmuir equation (figure 3.17 – figure 3.19).

Table 4: Value of the Langmuir constants

adsorbent	Temp. (K)	q_m	K_L	R^2
Cysteine-coated Fe_3O_4	308	32.23	3.8024	0.9855
	313	30.29	2.0347	0.9789
	318	37.35	1.144	0.9883

These plots show the linear relationship between $1/qe$ and $1/C_e$ at different temperature with varying concentration such as, 5, 10, 15, 20, 25, 30 ppm.

$$y = 0.0073x + 0.032$$
$$R^2 = 0.9822$$
at Tem. 308K
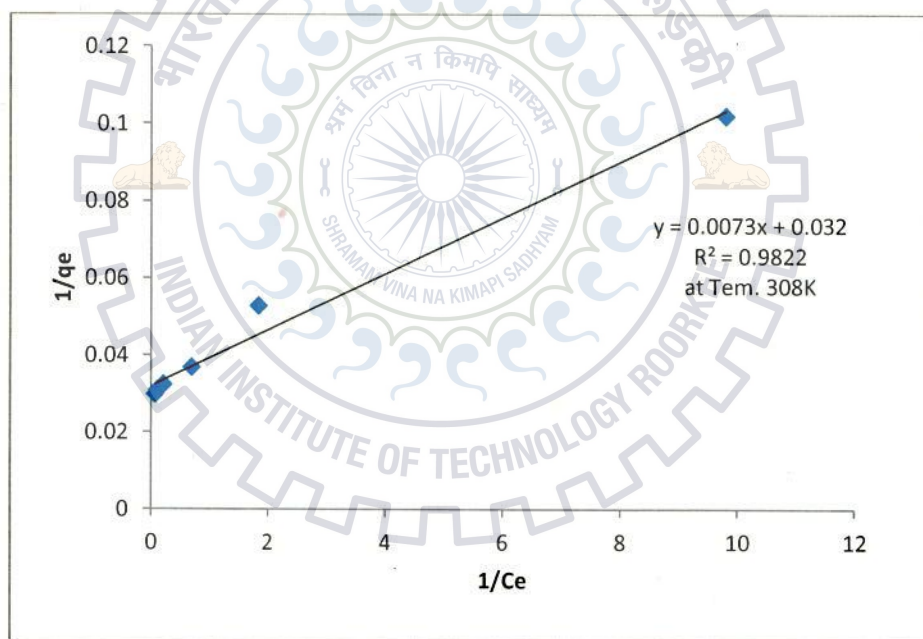
Figure 3.17: Langmuir isotherm for adsorption of Pb^{+2} onto Cysteine coated - Fe_3O_4 nanoparticles (0.5 g/L) at 308K and pH 6.
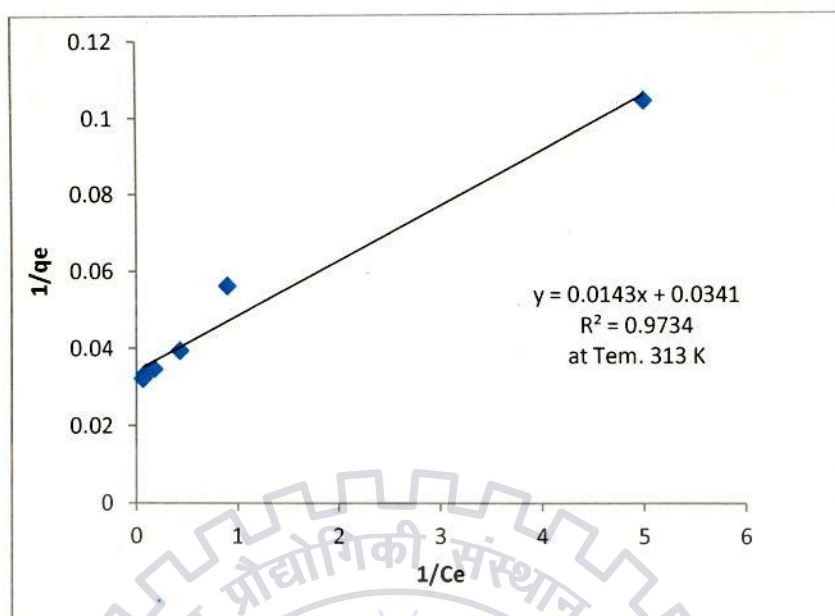
Figure 3.18: Langmuir isotherm for lead adsorption onto Cysteine coated - Fe_3O_4 nanoparticles, 0.5 g/L at 313K and pH 6.
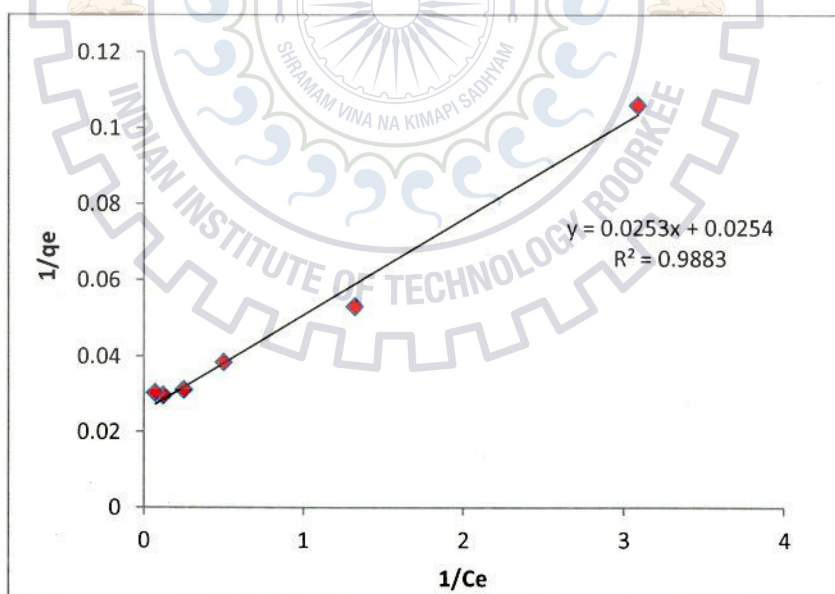
Figure 3.19: Langmuir isotherm for lead adsorption onto Cysteine coated - Fe_3O_4 nanoparticles, 0.5 g/L at 318K and pH 6

Thermodynamic studies:

From the Langmuir curves obtained at three temperatures, Thermodynamic parameters such as Gibbs free energy (ΔG°), enthalpy (ΔH°) and entropy (ΔS°) were calculated using the equations:

$$\Delta G^\circ = -RT \ln b$$

$$b = \frac{\text{Intercept of the straight line}}{\text{Slope of the straight line}}$$

The slop of straight line in the above plot gives the value of b.

$$\frac{\Delta G^\circ}{T} = \frac{\Delta H^\circ}{T} - \Delta S^\circ$$

Where R is the gas constant ($8.314 \ \text{J.mol}^{-1}\text{K}^{-1}$), Temperature is represents in Kelvin (K) and constant b was calculated by the slope. Langmuir constants (K_L and q_m) can be obtained by the equilibrium studies. And enthalpy (ΔH°) is determined using below given relation. Assuming ΔH° remains constant within the given temperature range. The value of ΔH° and ΔS° was determined by the Vant Haff plot between ln b and 1 / T. By the slop and intercept of the Vant Haff plot these values were find out.

$$\ln\left(\frac{b_2}{b_1}\right) = \frac{\Delta H^\circ}{R} \ [(1/T_2) - (1/T_1)]$$

The constant b is calculated by the slope of the linear plot on different temperature.

Adsorbent	Temp (K)	b	$\Delta G°$ (kJ mol^{-1})	$\Delta H°$ (kJ mol^{-1})	$\Delta S°$ (kJ mol^{-1})
Cysteine coated - Fe$_3$O$_4$	308	4.383	-3.784	121.8	0.38
	313	2.3846	-2.261		
	318	1.0039	-0.0102		

For all the temperatures, the Gibb's free energy ($\Delta G°$) is negative. It means that the adsorption process is spontaneous with high preference of lead for all adsorbents. The value of enthalpy is positive which shows the adsorption process is endothermic. The positive value of entropy 0.38 kJ mol^{-1} shows the higher randomness tendency at the adsorbent and adsorbates interface during lead adsorption onto the nanoparticles. Based on thermodynamics, negative value of $\Delta G°$ and positive value of $\Delta H°$ and $\Delta S°$ give a spontaneous process at high temperature.

Desorption experiment:

Desorption experiment was done at two conditions at higher temperature and at low pH, an increase in temperature did not enhanced desorption appreciably. However, the effect of pH investigated in the present work guided as to explore low pH for desorption (Table 2). Indeed, at low pH approximately 82.5 ± 7.5 % metal recovery occurred. This experiment was done with 10 ppm of Pb(NO$_3$)$_2$.

Conclusion

In summary we have successfully synthesize cysteine coated - Fe_3O_4 nanoparticles in which Fe_3O_4 is present in the core. In this nanosystem Fe_3O_4 is found to have inverse spinel structure as we arrived by XRD and SAED analysis. Fe_3O_4 nanoparticles is observed to interact with cysteine through its –SH and –COO^- groups which also caused a shift in absorption due to different functionality of cysteine. Optical spectroscopy also indicates an interaction between Fe_3O_4 and cysteine, which shows a red shift in absorption due to cysteine associated with the reduction in intensity of a broad absorption due to Fe_3O_4 nanoparticles. These coated particles found to have an average size 12 nm. As expected, the coating of these particles caused a decrease in magnetization of the coated particles as compare to Fe_3O_4 nanoparticles. Cysteine coated Fe_3O_4 nanoparticles were found to efficiently adsorb Pb^{+2}. The adsorption of Pb^{+2} follow the Langmuir isotherm within the concentration range from 5 to 30 ppm. Desorption of the adsorb Pb^{+2} could be carried out at low pH up to 82.5 ± 7.5 % a concentration with previously studies iron oxide based nanosystem. The adsorption capacity and desorption efficiency for this system are encouraging and need to be further analyzed with this and another related metal ion.

CHAPTER - 4

REFERENCES

1. Klabunde K. J. and Richards, R.M., *Nanoscale Materials in Chemistry*, **2009**, Ed – Second, John Wiley & Sons.

2. Blanco-Andujar, C.; Tung, L. D. and Thanh, T. K., *Annu. Rep. Prog. Chem. Sect. A*, **2010**, 106, 553-568.

3. Pankhurt, Q. A.; Connolly, J.; Jones, S.K. and Dobson, J., *J. Phys. D: Appl. Phys.*, **2003**, 36, R167 - R187.

4. Tiwari, D. K.; Behari, J. and Sen, P., *World Appl. Sci. J.*, **2008**, 3(3), 417-433.

5. Sass, Jennifer; *NRDC issue Paper –Natural Resources Defence Counsil*, **2007**.

6. Gupta, A.K. and Gupta, M., *Biomaterials*, **2005**, 26, 3995-4021.

7. Romanus, E.; Huckel, M.; Grob, C.; Prass, S.; Weitschies, W.; Brauer, C. and Waber, P., *J. Magnetism and Magnetic Material*, **2002**, 252, 387-389.

8. Latorre, M and Rinaldi, C.; *Magnetic Fluid Hyperthermia-PRHSJ*, **2009**, 28 (3), 227-238.

9. Mahmoudi, M.; Sant, S.; Wang, B.; Laurent, S. and Sen, T., *Advanced Drug Delivery Reviews*, **2011**, 63, 24-46.

10. Gee, S.H.; Hong, Y.K.; Erickson, D.W. and Park, M.H., *J. Applied Physics*, **2003**, 93(10), 7560-7562.

11. Shokouhimehr, M.; Piao,Y.; Kim, J.; Jang Y. and Hyeon, T., *Angew. Chem. Int. Ed.*, **2007**, 46, 7039-7043.

12. Hua M., Zhang S., Pan B., Zhang W., Lv L. and Zhang Q.; *J. Hazardous Materials*, 211-212, 317-331, 2012.

13. Qiao, R.; Yang, C. and Gao, M., *J. Materials Chemistry*, **2009**, 19, 6274-6293.

14. Yu, M.; Huang, S.; Yu, K.J. and Clyne, M., *Int. J. Mol. Sci.*, **2002**, 13, 5554 – 5570.

15. Lee, H.Y.; Lee, S.H.; Xu, C.; Xie, J.; Lee, J.H.; Wu, B.; Koh, A.L.; Wang, X.; Sinclair, R.; Wang, S.X.; Nishimura, D.G.; Biswal, S.; Sun, S.; Cho, S.H.; and Chen, X., *Nanotechnology*, **2008**, 19 (16), 1-14.

16. Liu, J.F.; Zhao, Z.S. and Jiang, G.B., *Environ. Sci. Technol.*, **2008**, 42, 6949-6954.

17. Chen, Y.; Hu, J.; and Wang, J., *Environmental Technology iFirst*, **2012,** 1-7.

18. Chou, C.M.; and Lien, H.N., *J. Nanopart. Res.*, **2011**, 13, 2099-2107.

19. Roqua, C.A.A.; Bicho, A.; Batalha, I.L.; Cardoso, A.S.; and Hussian, A., *J. Biotechnology*, **2009**, 144, 313-320.

20. Madrakian, T.; Afkhami, A.; Zolfigol, M. A.; Ahmadi, M. and Koukabi, N., *Nano-micro Lett.*, **2012,** 4(1), 57-63.

21. An, B.; Liang, Q. and Zhao, D., *Water Research*, **2011**, 45, 1961-1972.

22. Yang, H.M.; Lee, H.J.; Jang, K.S.; Park, C.W.; Yang, H. W.; Heo, W.D. and Kim, J.D., *J. Materials Chemistry*, **2009**, 1-8.

23. Huang, J.; Wang, L.; Lin, R.;Wang, A.Y.; Yang, L.; Kuang, M.; Qian, W. and Mao, H., *Appl. Mater. Interfaces*, **2013**, 5, 4632 – 4639.

24. Woo, K.; and Hong, J., *IEEE Ttransaction on Magnetic*, **2005**, 41(10), 4137-4139.

25. Rao, V.; Shahimohan, A.L. and Biswas, A.B., *J. Materials Science*, **1974**, 9, 430-433.

26. Sahoo, S.K.; Agarwal, K.; Singh, A.K.; Polke, B.G. and Raha, K.C., *Inertna. J. Engg.,Sci., Techno.*, **2010**, 2(8), 118-126.

27. Lu, A. H.; Salabas, E. L. and Shuth, F., *Angew. Chem. Int. Ed.*, **2007**, 46, 1222-1244.

28. Mohapatra, M. and Anand, S., *Interna. J. Engg. Scien. Tech.*, **2010**, 2(8), 127-146.

29. Xu, P.; Zeng, G. M.; Huang, D. L.; Feng, C. L.; Hu, S.; Zhao, M. H.; Lai, C.; Wei, Z.; Huang, C.; Xie, G. X. and Hu, Z. F., *Science of the total environment*, **2012**, 424, 1-10.

30. Vaishya, R. C. and Gupta, S. K., *J. Chem. Technol. Biotechnol.*, **2002**, 78, 73-80.

31. Feng, Z.; Zhu, S.; Godoi, D.R.M.D.; Samia, A.C.S.S. and Scherson, D., *Anal. Chem.*, **2012**, 84, 3764 - 3770.

32. Parham, H.; Zargar, B. and Shiralipour, R., *J. Hazardous Material*, **2012**, 205-206, 94-100.

33. Sampranpiboon, P. and Carnkeitkong, P., *Int. J. Energy and Environment*, **2010**, 4 (3), 88 – 95.

34. Wang, J.; Zheng, S.; Shao,Y.; Liu, J.; Xu, Z. and Zhu, D., *J. Colloid and Interface Science*, **2010**, 349, 293-299.

35. Ge, F.; Li,M. M.; Ye,H. and Zhao,B.X, *J. Hazardous Materials*, **2012**, 211-212, 366-372.

36. Chen, R.; Zhi, C.; Yang, H.; Bando, Y. Zhang, Z.; Sugiur, N. and Golbery, D., *J. Colloid and Interface Science*, **2011**, 390, 261-268.

37. Badruddoza, A.Z.M.; Tay, A.S.H.; Hidajat, K. and Uddin, M.S., *J. Hazardous Materials*, **2011**, 885, 1176-1186.

38. White, B.R.; Stackhouse, B.T. and Holcombe, J.A., *J. Hazardous Materials*, **2009**, 161, 848-853.

39. Ahmadi, R.; Malek, M.; Hosseini, H.R.M.; Shokrgozar, M.A.; Oghabian, M.A. and Masoudi, A.; Zhang, Y., *J. Materials Chemistry and physics*, **2011**, 131, 170-177.

40. Ahmedi, R. and Gu, Ning, *Nano-Micro Lett.*, **2012**, 4(3), 180-183.

41. Yang, Z.; Dai, P. and You, Y., *Microchim. Acta.*, **2012**, 477, 449-456.

42. Cullity, B.D., *Element of X-ray Diffarction*, **1956**, *Addition – Wesley Publishing, Company, Inc.,*.

43. Foner, S., *The Review of Scientific Instrument*, **1959**, 30 (7), 548-557.

44. Chatterjee, S.; Gadad, S.S. and Kundu, K., *Resonance*, **2010**, 622 – 642.

45. Goohew, P.J.; Humphreys, J. and Beanland, R., *Electron Microscopy and Analysis*, **2001**, Ed.-Third, Taylor and Francis.

46. Rouessac, F. and Rouessac, A., *Chemical Analysis*, **2007**, Ed – Second, John Wiley & Sons.

47. Kemp, W., *Organic Spectroscopy*, **1991**, Ed – Third, Palgrave.

48. Skoog, D.A.; Holler, F.J. and Crouch, S.R., *Instrumental Analysis*, **2007**.

49. Gawande, M.B.; Velhinho, A.; Nogueira, I.D.; Ghumman, C.A.A.; Teodoro, O.M.N.D. and Branco, P.S., *RSC Advances*, **2012**, 6144 – 6149.

50. Lewinsky, A.A., *Hazardous Material and Waste Water: Treatment, Removal and Analysis*, **2007**, New York, N Y: Nova Science.